Functional interplay of Epstein-Barr Virus oncoproteins in a mouse model of B cell lymphomagenesis

Thomas Sommermann[1,*], Tomoharu Yasuda[1,7], Jonathan Ronen[6,7], Tristan Wirtz[1], Timm Weber[1], Ulrike Sack[1], Rebecca Caeser[2], Jingwei Zhang[1], Xun Li[1], Van Trung Chu[1,3], Anna Jauch[4], Kristian Unger[5], Daniel Hodson[2], Altuna Akalin[6] and Klaus Rajewsky[1,8,*]

1 Department of Cancer Research, Max-Delbrück Center for Molecular Medicine, Berlin,13215, Germany

2 Welcome-MRC Cambridge Stem Cell Institute, Department of Haematology, University of Cambridge, Cambridge, CB2 0AF, UK

3 Berlin Institute of Health, Berlin, 10178, Germany

4 Institute of Human Genetics, University Heidelberg, Heidelberg, 69120, Germany

5 Research Unit of Radiation Cytogenetics, Helmholtz Zentrum München, Neuherberg, 85764, Germany

6 Berlin Institute for Medical Systems Biology, Max-Delbrück Center for Molecular Medicine Berlin, 10115, Germany

7 These authors contributed equally

8 lead contact

** Correspondence: klaus.rajewsky.mdc-berlin.de and Thomas.sommermann@mdc-berlin.de*

Classification

Biological Sciences ; Microbiology

Keywords

Epstein-Barr Virus, LMP1, EBNA, B cell lymphomagenesis, plasma cell differentiation

Author Contributions

T.S. and K.R. conceived, designed and initiated the study. T.S. performed experiments. T.Y. performed Cγ1-Cre experiments. J.R. supervised by A.A. performed bioinformatic analysis. T.Y., T.W., T.W., V.T.C. and X.L. assisted T.S. in experiments. U.S. generated the R26BFP^{stopf} mouse. K.U. performed the array-CGH. A.J. performed the M-FISH. R.C. and J.Z. supervised by D.H. performed human GCB experiments. T.S. and K.R. prepared the manuscript. K.R. secured funding and supervised the work. The authors do not have competing interests.

Summary

Epstein-Barr Virus (EBV) is a B cell transforming virus that causes B cell malignancies under conditions of immune suppression. EBV orchestrates B cell transformation through its Latent Membrane Proteins (LMPs) and Epstein Barr Nuclear Antigens (EBNAs). We here identify secondary mutations in mouse B cell lymphomas induced by LMP1, to predict and identify key-functions of other EBV genes during transformation. We find aberrant activation of Early B Cell Factor 1 (EBF1) to promote transformation of LMP1-expressing B cells by inhibiting their differentiation to plasma cells. EBV EBNA3A phenocopies EBF1-activies in LMP1 expressing B cells, promoting transformation while inhibiting differentiation. In cells expressing LMP1 together with LMP2A, EBNA3A only promotes lymphomagenesis when the EBNA2-target Myc is also overexpressed. Collectively, our data support a model where pro-proliferative activities of LMP1, LMP2A and EBNA2 in combination with EBNA3A-mediated inhibition of terminal plasma cell differentiation critically control EBV-mediated B cell lymphomagenesis.

Significance statement

Epstein-Barr Virus (EBV) efficiently transforms human B cells and causes B cell lymphomagenesis especially in immunocompromised patients. We study this process in

genetically engineered mice to untangle the interplay of EBV oncogenes. We find Epstein Barr Nuclear Antigen (EBNA) 3A to have both oncogenic and tumor suppressive roles. First, EBNA3A promotes B cell transformation by inhibiting LMP-driven plasma cell differentiation, a function which can be mimicked by aberrant activation of Early B cell factor 1 (EBF1). Second, EBNA3A blunts Myc-driven proliferation, rendering B cell transformation dependent on Myc activation by the EBV protein EBNA2. The presented mouse model thus highlights the role of EBV oncogenes in orchestrating B cell transformation through control of B cell differentiation and MYC levels.

Introduction

Epstein Barr Virus (EBV) is a B-lymphotropic γ-herpesvirus that is endemic in humans, with more than 90% of the population latently infected (1). EBV is the only known virus capable to in vitro transform human B cells into continuously proliferating lymphoblastoid cell lines (LCLs). In healthy individuals proliferating EBV-infected B cells are eliminated by a T and NK cell mediated immune response, restricting infection to rare memory B cells with no or limited viral gene expression (2). Immunocompromised patients fail to control infected B cells and are thus prone to develop EBV^+ B cell pathologies (2). A prominent example are EBV^+ post-transplant lymphoproliferative disorders (PTLDs) arising in up to 22% of patients undergoing immunosuppressive drug treatment after organ transplantation (3). EBV^+ PTLDs present as polymorphic or monomorphic disease, the latter mostly resembling Activated B Cell-Like (ABC)-DLBCL and less frequently, Hodgkin- (HL) or Burkitt-lymphoma (BL) or plasma cell neoplasms (3). PT-ABC-DLBCLs usually express the EBV growth program (called latency III) which also facilitates B cell to LCL transformation in vitro, suggesting that EBV is the main driving force in such tumors (1, 4). The EBV growth program involves expression of several non-coding RNAs, three Latent Membrane Proteins (LMPs) and seven Epstein Barr Nuclear Antigens (EBNAs) (1). LMPs and EBNAs were shown to control key steps of B cell activation: LMP1 mimics an active CD40 receptor to mainly induce NF-κB and JNK signaling pathways (5,

6). LMP2A resembles a constitutively active B cell receptor (BCR), primarily activating PI3K and MAPK signaling (7–9). EBNA2 mimics NOTCH in binding to RBP-J and activating target genes, most notably *MYC* (10). EBNA3A and 3C also bind RBP-J but serve as transcriptional repressors, epigenetically silencing the tumor suppressor genes *CDKN2A* (p16-INK4a/ARF) and *BCL2L11* (BIM) (11). Despite ample work on the activity of LMPs and EBNAs during in vitro transformation, their impact on B cell lymphomagenesis in vivo remains elusive. This is largely due to EBV not infecting small laboratory animals (12). Furthermore, modeling EBV-pathologies in transgenic mice had a limited success, with only LMP1-transgenic mice showing reliable B cell tumor development at old age (8, 13–18). More recently, EBV-infection in mice reconstituted with human hematopoietic cells is successfully used to recapitulate virally-driven B cell lymphomagenesis (19), yet this approach like the transformation of human B cells in vitro relies on infectious EBV, making it challenging to study the activity of single LMP or EBNA genes.

We previously developed a conditional transgenic mouse model that recapitulates EBV-driven lymphomagenesis in immunodeficient hosts (20). In this model, B cell specific activation of a Rosa26 (R26) LMP1-transgene induces B cell proliferation followed by their T cell-mediated elimination. In T cell-deficient mice LMP1-expressing B cells (LMP1 B cells) cause a lymphoproliferative disease (LPD) that within few months spontaneously progresses to lymphoma. Strikingly, such LMP1-driven lymphomas (LMP1-Ls) are monoclonal, arguing that spontaneous somatic mutations are required to transform LMP1 B cells. We set out to identify such mutations in order to define pathways that must be engaged by EBV for successful B cell transformation. A recurrent activating mutation of the B cell transcription factor EBF1 turned out to be a functional proxy of the EBV gene EBNA3A in its interplay with other EBV oncogenes in B cell transformation.

Results

Ebf1 and Rel are aberrantly activated in mouse LMP1-Lymphomas

Previously established LMP1-Ls were created on a mixed genetic background and without a reporter, rendering it challenging to prepare pure lymphoma samples for genetic analysis (20). We here combined a *R26LMP1-ires-huCD2*^{stopf} allele (*R26LMP1*^{stopf}) (21) with *Cd3ε*^{KO} to confer T cell deficiency and *Cd19-Cre* for B cell specific deletion of the floxed stop-cassette (stopf) to allow LMP1 and huCD2-reporter expression on a C57BL/6 background. To create a lymphoma cohort, we transplanted fetal liver hematopoietic stem and progenitor cells (fHSPC) from *Cd3ε*^{KO}*;Cd19-Cre;R26LMP1*^{stopf} mice into irradiated *RAG2*^{KO}*cγ*^{KO} mice (tpLMP1 mice) (Fig. 1A). Within 7 months all tpLMP1 mice developed LMP1-Ls infiltrating liver, lung and spleen (Fig. 1B, S1A). In line with previous findings (20), histologic analyses graded LMP1-Ls as CD10^{-}, BCL6^{-} and MUM1^{+} (Fig. S1A, Table S1), resembling ABC-DLBCL (22). To separate LMP1-L cells from non-transformed LMP1 B cells (tpLMP1 B cells), we transplanted 5x10^{6} cells from tpLMP1 mice with primary tumors into secondary immunodeficient recipients. All secondary (2^{ry}) LMP1-Ls were CD19^{+}, expressed the LMP1 target FAS and a single immunoglobulin (Ig) isotype (Fig. S1B, Table S1). Southern blot analysis for Ig-heavy chain rearrangements confirmed B cell origin and clonality of 2^{ry}LMP1-Ls (Fig. S1C). To define somatic driver mutations, we performed exome sequencing on 10 sorted 2^{ry}LMP1-Ls. Tumors harbored between 16 and 60 clonal mutations (Fig. S1D, Table S2). Mutations mostly altered non-coding regions. Mis- or nonsense mutations were rare and never involved the same protein coding sequence in independent tumors. As exome-sequencing did not reveal obvious candidates for driver mutations, we performed array-CGH to detect chromosomal aberrations. Besides expected copy number variations (CNV) in the Ig-loci on Chr6 (*Igk*) and Chr12 (*Igh*), the most common CNVs were complete or partial gains of Chr11 and Chr15 (Fig. S1E, Table S3). Interestingly, lymphomas 37 and 43 shared a copy number loss 3' of the IgH-locus on Chr12 and a partial copy number gain of Chr11 (Fig. S1E, S1F), a pattern indicative of a non-balanced translocation between the respective loci

(23). Indeed, M-FISH analysis of LMP1-L-derived cell lines (LMP1-CL) confirmed t(11;12) translocations in tumors 37 and 43 (Fig. 1C, S1G, Table S4). Chimeric reads involving the Ig-loci in exome sequencing and subsequent Sanger-sequencing of the chimeric locus in primary LMP1-Ls mapped the exact translocation in tumor 43 to *Ighe*-exon 3 and intron 9 of *Rnf145*, 57kb upstream of the *Ebf1* gene (Fig. 1D, S1H, S1I Table S5). Exome sequencing reads did not span the translocation site in tumor 37, but revealed a translocation in 2^{ry}LMP1-L 31 involving the Igκ-locus on Chr6 and Chr11 25kb upstream of *Rel* (encoding NF-κB transcription factor c-Rel) (Fig. 1D, S1H, S1I, Table S5). As translocation of genes into the proximity of Ig-enhancers is a common mechanism to activate oncogenes in B cell tumors (24), we determined *Ebf1*- and *Rel*-expression by RNA-sequencing of tpLMP1 B cells before and after transformation. Compared to naive B cells from C57BL/6 mice, non-transformed tpLMP1 B cells showed reduced expression of *Ebf1* and *Rel* (Fig. 1E). In contrast, all 2^{ry}LMP1-Ls overexpressed one of the two genes, with t(11;12)-translocated tumors 37 and 43 expressing elevated *Ebf1*-levels (Fig. 1E). Corresponding to the RNA-expression levels in the initial tumor, LMP1-CLs expressed elevated protein levels of EBF1 or c-Rel (Fig. S1J). LMP1-CL 45 highly expressed c-Rel and EBF1, although the initial tumor was *Ebf1*^{high}/*Rel*^{low}. Taken together, *Ebf1* and *Rel* are recurrently activated in LMP1-Ls and were thus considered as secondary driver candidates. In non-supervised principle component analysis on global RNA-expression *Ebf1*- and *Rel*-expression formed separate tumor subgroups, further indicating that both genes define distinct LMP1-L subsets (Fig. 1F).

Ebf1- or Rel-overexpression supports transformation of LMP1 B cells

To analyze the impact of LMP1/EBF1 or LMP1/c-Rel co-expression on naïve B cells, we isolated CD43^{-} B cells from *R26LMP1*^{stopf} mice and induced LMP1-expression in vitro (iLMP1 B cells) by incubating the cells with HIV-TAT-coupled Cre-recombinase (TAT-Cre) (Fig. 2A). One day after TAT-Cre, iLMP1 B cells were transduced with retroviruses (RV) encoding *GFP*, *Ebf1* or *Rel*. Control-transduced iLMP1 B cells transiently expanded for 8-10 days (Fig. 2B). Strikingly, *Ebf1*- or *Rel*-transduced iLMP1 B cells continued to

expand and turned into continuously proliferating mouse lymphoblastoid cell lines (EBF1-LCL, c-Rel-LCL) (Fig. 2B). *Ebf1* or *Rel* expression in anti-CD40 (αCD40)/IL-4 stimulated control B cells did not promote proliferation. After 45 days PCR-analysis for diversity of VDJ-rearrangements indicated oligoclonal outgrowth of EBF1-LCLs and c-Rel-LCLs (Fig. S2A). Like human LCLs, these mouse LCLs aggregated in clumps and expressed the surface markers CD19, CD20, MHCII, Ig-light chain, ICAM and FAS (Fig.S2B, Table S6) (25, 26). Also similar to human LCLs, CD23 was expressed only in a subset of mouse LCLs. CD3ε (not expressed on LCLs) was expressed at low levels on 1 out of 4 analyzed EBF1-LCLs. EBF1-LCLs could be grown from ~2% of single-sorted *Ebf1*-tranduced iLMP1 B cells, while c-Rel-LCLs rarely grew as single cell clones (Fig. 2C). To validate their malignancy, $3x10^5$ freshly *Ebf1*- or *Rel*-transduced iLMP1 B cells were transferred into $Rag2^{KO}c\gamma^{KO}$ mice. Within 12-21 days all transplanted mice developed severe lymphoproliferative disease (Fig. 2D), with *Rel*- or *Ebf1*-expressing iLMP1 B cells expanding in liver and spleen (Fig. 2E-G). Analysis for VDJ-diversity did not indicate clonal selection in this timeframe (Fig. S2C). Indeed, transfer of as few as $1x10^3$ *Ebf1*- or *Rel*-transduced iLMP1 B cells caused terminal lymphoproliferative disease within approximately 30 (LMP1/EBF1) or 60 days (LMP1/c-Rel) (Fig. 2D). Taken together, aberrant expression of *Ebf1* or *Rel* leads to an efficient transformation of mouse LMP1 B cells in vivo and in vitro. To determine whether combined LMP1/EBF1 or LMP1/c-Rel expression also supports expansion of human B cells, we made use of a recently published system to transduce primary human tonsillar GCBs (27). While single transduction of *Ebf1 or Rel* had little impact on human GCBs, EBF1 and, to a minor extent c-Rel, indeed enhanced the expansion of LMP1-expressing GCBs (Fig. 2H).

Rel-activation induces LMP1/NF-κB-target genes

Rel overexpression in LMP1-Ls should elevate NF-κB target gene expression through increased nuclear c-Rel. Indeed, secondary Rel^{high} LMP1-Ls and the *Rel/Igk* translocated lymphoma 31 expressed more (mostly nuclear) c-Rel than non-transformed tpLMP1 B cells and $Ebf1^{high}$ LMP1-Ls (Figure S3A). Furthermore, in our RNA-sequencing data, a

set of previously described human LMP1/NF-κB target genes (26) was significantly more highly expressed in *Rel*^{high} 2^{ry}LMP1-Ls compared to *Ebf1*^{high} 2^{ry}LMP1-Ls and tpLMP1 B cells (Fig. S3B, S3C). Among these genes were the anti-apoptotic Bcl2-family members *Bcl2l1* (Bcl-X), *Bcl2a1a* and *Bcl2a1d* (BFL-1a/d) (Fig. S3D), which may well support B cell transformation.

Ebf1 inhibits plasma cell differentiation of LMP1 B cells

EBF1 is a transcription factor that is required to maintain B cell identity (28). During plasma cell (PC)-differentiation *Ebf1* expression is silenced (29). As LMP1 suppressed *Ebf1* transcription (Fig. 1E), we wondered whether LMP1 induces B cell differentiation towards PCs. Indeed, compared to naïve splenic B cells tpLMP1 B cells showed low expression of the B cell transcription factor genes *Pax5*, *Ets1*, *Bcl6* and *Bach2* and elevated transcription of the master PC transcription factor gene *Prdm1* (Fig. 3A). Furthermore, tpLMP1 B cells expressed the PC-surface marker CD138 (Fig. 3B, 3D). In contrast, *Ebf1*^{high} LMP1-Ls showed neither CD138 surface-staining nor elevated levels of *Prdm1* mRNA (Fig. 3A, 3C, 3D). To test whether *Ebf1*-induction is sufficient to block LMP1-mediated PC-differentiation in vitro, we performed RNA-sequencing on retrovirally transduced iLMP1 B cells. *Ebf1*-overexpression blunted *Prdm1* induction and shifted the global mRNA expression pattern of iLMP1 B cells from PC- to GCB-like (Fig. 3E-F). *Ebf1*-overexpression also blunted plasma blast (PB)-differentiation of naïve B cells cultured on CD40-L and BAFF expressing feeders (40LB) (30) (Fig. S3E-F). Despite recent reports that c-Rel can suppress PC-differentiation (31), *Rel*-overexpression had little impact on *Prdm1* expression in iLMP1 B cells and did not inhibit PB-differentiation of cytokine stimulated wild type B cells (Fig. 3E, S3E-F). Furthermore, *Ebf1*- but not *Rel*-overexpression blunted PB-differentiation of iLMP1 B cells when transplanted into *RAG2*^{KO}*c*γ^{KO} mice (Fig. S3G). GFP control transduced cells did not survive long enough after transplantation to be analyzed. Although c-Rel alone did not impact PB-differentiation, the majority of *Rel*^{high} LMP1-Ls showed low or no CD138 expression (Fig. 3D), arguing that *Rel*^{high} LMP1-Ls also benefit from a loss of PC-differentiation. Taken

together, loss of PC-differentiation is a general feature of LMP1-driven lymphomagenesis, caused either by EBF1-activation or unknown events in the *Rel*^{high} cases. Importantly, suppression of PC-differentiation is considered to be a key event in NF-κB-driven ABC-DLBCL development (32), suggesting that EBF1-suppressive effects on LMP1-induced PC-differentiation are critical for the transformation of LMP1 B cells to DLBCL-like tumors.

EBNA3A inhibits PC-differentiation in transgenic mice

We next set out to define EBV growth program genes whose role in transformation and differentiation might be mimicked by aberrant EBF1-activation. As LMP2A, unlike EBF1, was reported to promote PC-differentiation (33) we focused on EBNA genes. To determine their impact on LMP1-driven transformation we retrovirally overexpressed individual HA-tagged EBNAs in iLMP1 B cells. EBNA2 expression was below the detection limit and could therefore not be studied (Fig. S4A). All other EBNAs were readily detectable in the nucleus of transduced iLMP1 B cells, but only EBNA3A supported cell expansion (Fig. 4A, S4A). To study EBNA3A in vivo we generated a *R26CAG-EBNA3A-HA-ires-BFP*^{stopf}-allele (*R26EBNA3A*^{stopf}) and a *R26CAG-BFP-ires-huCD2*^{stopf} reporter-allele (*R26BFP*^{stopf}) (Fig. S4B-C). Both novel R26-alleles were combined with *Cd19-Cre*$^{cre/+}$ *(Cd19-Cre)* for B cell specific transgene expression. *Cd19-Cre;R26EBNA3A*^{stopf} and *Cd19-Cre;R26BFP*^{stopf} mice expressed the BFP-reporter in the majority of (CD19$^+$B220$^+$) splenic B cells (Fig. 4B). HA-co-immunoprecipitation experiments in αCD40/IL-4 stimulated splenic B cells confirmed EBNA3A-protein expression in *Cd19-Cre;R26EBNA3A*^{stopf} B cells and conserved EBNA3A-binding to its core interaction partner RBP-J (Fig. S4D). *Cd19-Cre;R26EBNA3A*^{stopf} and *Cd19-Cre;R26BFP*^{stopf} mice had a normal life expectancy (Fig. 4C). Furthermore, EBNA3A-expression in B cells did not impact splenic size, cellularity and absolute B cell numbers (Fig. S4E). *Cd19-Cre; R26EBNA3A*^{stopf} mice had a normal frequency of BFP$^+$ pro-, pre- and immature B cells in the bone marrow, while the frequency of reporter$^+$ mature B cells in the spleen was mildly reduced (Fig. 4D), an effect at least partially attributable to limited separation of BFP$^+$ and BFP$^-$ B cells. Although their number was almost normal, EBNA3A$^+$ splenic B cells showed a disturbed marginal zone B cells (MZB) and follicular B cells (FOB) surface staining, with

$CD23^{low}CD21^{+}$ MZBs being absent and numbers of $CD23^{+}CD21^{low}$ FOBs being reduced (Fig. S4F). Instead, most $EBNA3A^{+}$ B cells were $CD23^{low}CD21^{low}$. Despite these alterations, all $EBNA3A^{+}$ cells expressed surface IgM and IgD levels similar to FOBs (Fig. S4F). Also, spleens of *Cd19-Cre;R26EBNA3A*^{stopf} mice had a normal follicular structure including $EBNA3A^{+}$ B cells locating to B cell follicles and the marginal zone (Fig. S4G). Although EBNA3A was expressed in more than 80% of mature splenic B cells, $CD138^{+}CD267^{+}$ PCs of *Cd19-Cre;R26EBNA3A*^{stopf} mice rarely expressed EBNA3A (Fig. 4E). Furthermore, the frequency of antibody secreting cells (ASC) among BFP^{+} cells in the bone marrow of *Cd19-Cre;R26EBNA3A*^{stopf} mice was more than 7-fold reduced compared to *Cd19-Cre;R26BFP*^{stopf} mice (Fig. 4F). To address whether $EBNA3A^{+}$ B cells can differentiate in vitro, we cultured BFP^{+} FOBs from *Cd19-Cre;R26EBNA3A*^{stopf} and *Cd19-Cre;R26BFP*^{stopf} mice on 40LB feeders. While FOBs from control mice readily differentiated into $CD138^{+}$ plasma blasts, the majority of $EBNA3A^{+}$ FOBs remained $CD138^{-}$ (Fig. S4H). Importantly, αCD40/IL-4 stimulated FOBs from *Cd19-Cre;EBNA3A*^{stopf} mice expanded better than control cells, arguing that CD40-signaling in $EBNA3A^{+}$ B cells is rather elevated than impaired (Fig. S4I). Similarly, LPS and IL-4 stimulation did not induce PC-differentiation of $EBNA3A^{+}$ FOBs (Fig. S4J). Taken together, EBNA3A expression in mouse B cells does not promote lymphomagenesis, has little impact on early B cell development, distorts differentiation of mature B cell subsets (at least at surface marker level) and strongly inhibits terminal PC-differentiation.

EBNA3A inhibits PC-differentiation and supports expansion of LMP1 B cells

To evaluate the impact of EBNA3A on proliferation and differentiation of LMP1 B cells, we isolated B cells from *R26LMP1*^{stopf}*;R26EBNA3A*^{stopf} mice and activated transgene expression by TAT-Cre treatment (iLMP1/EBNA3A B cells). iLMP1/EBNA3A B cells expanded more than iLMP1 B cells, with EBNA3A supporting cell proliferation and inhibiting apoptosis (Fig. 5A-C). RNA-sequencing on day 6 revealed attenuated *Prdm1* expression in iLMP1/EBNA3A B cells (Fig. 5D). This effect was independent of *Ebf1*, as EBNA3A did not restore *Ebf1* expression in these cells. In human B cells *CDKN2A* and *BCL2L11* are considered as EBNA3As key target genes (11). In iLMP1/EBNA3A B cells,

EBNA3A severely blunted LMP1-induced *Cdkn2a* expression, while the impact on *Bcl2l11*-levels was more modest (Fig. S5A, S5B). Yet, deleting *Cdkn2a*- or *Bcl2l11*-ORFs by retroviral delivery of sgRNAs into iLMP1/CAS9 B cells did not promote cell expansion (Fig. S5C, S5D), arguing that EBNA3A-function extends beyond the suppression of *Cdkn2a* or *Bcl2l11*.

To test the impact of combined EBNA3A and LMP1 expression on B cells in vivo, we transplanted *Cd3ε^{KO};Cd19-Cre;R26LMP1^{stopf};R26EBNA3A^{stopf}* fHSPCs into irradiated *RAG2^{KO}cγ^{KO}* mice (tpLMP1/EBNA3A). In contrast to tpLMP1 mice, tpLMP1/EBNA3A mice developed terminal LPD within 40 days after reconstitution (Fig. 5E). Spleens of tpLMP1/EBNA3A mice were dramatically enlarged and filled with LMP1$^+$/EBNA3A$^+$ B cells (Fig. 5F, 5G, S5E). Analysis of VDJ-rearrangements in splenocytes of tpLMP1/EBNA3A mice did not indicate clonal B cell expansion at termination (Fig. S5F). Compared to tpLMP1 B cells tpLMP1/EBNA3A B cells showed reduced CD138 expression and antibody secretion (Fig. 5G, 5H, S5E). Thus, EBNA3A, like EBF1, facilitates polyclonal expansion of LMP1 B cells while inhibiting their differentiation to PBs, suggesting that EBNA3A substitutes for EBF1 during EBV-driven PTLD-development.

EBF1 and REL expression in human PT-DLBCLs

Given the impact of c-Rel and EBF1 on LMP1-driven B cell in the mouse model, we wondered whether LMP1 expression in human PT-DLBCLs positively correlates with *REL* activation, while *EBF1* might be specifically upregulated in LMP1$^+$/EBNA3A$^-$ cases. Alternatively, the presence of the full EBV-genome in the human disease might alleviate the need for *REL* or *EBF1* activation. We therefore correlated expression of *EBF1* and *REL* with EBV-infection and -latency status in a published human PT-ABC-DLBCL dataset (34). PT-DLBCLs datasets comparing exome-mutations and amplifications were either too small to be informative (37), or did not report EBV latency II cases (38–40), datasets reporting unbiased translocations in PT-DLBCLs were not available. In the expression analysis, latency II PT-ABC-DLBCLs (LMP1/2a;EBNA1) expressed rather less *EBF1* than latency III cases (LMP1/2a;EBNA1/LP/2/3A-C) (Figure S5G), arguing that

the absence of EBNA3A in latency II tumors does not commonly entail EBF1 activation. Furthermore, *REL*-levels, in line with other reports (35, 36), appeared independent of EBV infection (Figure S5G). Together these data suggest that the presence of the EBV genome alleviates the need for *REL* or *EBF1* activation in human PT-ABC-DLBCLs.

EBNA3A inhibits PC-differentiation of LMP1 and LMP2A expressing B cells

In the EBV growth program LMP1 and EBNA3A are co-expressed with LMP2A, which by itself promotes proliferation and PC-differentiation of LMP1 expressing mouse GCBs (41, 42). To evaluate whether lymphomagenesis of GCB cells expressing both LMPs also requires disruption of PC-differentiation, we transferred $3x10^6$ B cells from *Cγ1-Cre* (GCB-specific) *R26LMP1^{stopf};R26LMP2A^{stopf}* mice into *RAG2^{KO}* mice (Fig. 6A). Transferred cells contained merely 100-300 LMP1$^+$/2A$^+$ GCBs as these cells are continuously eliminated by T cells (Fig. 6B). In the reconstituted mice, LMP1$^+$/2A$^+$ GCBs proliferated strongly and overwhelmingly differentiated into CD138$^+$CD19^{low} PCs within 17-28 days (Fig. 6B, S6A). When aged, the reconstituted mice developed CD19$^+$CD138$^-$LMP1$^+$/2A$^+$ B cell lymphomas (Fig. 6C-E). One mouse developed a CD19$^+$CD138$^-$LMP1$^+$/2A$^-$ B cell lymphoma (Fig. S6B). Thus, upon transfer into an immunodeficient environment, LMP1$^+$/2A$^+$ GCBs proliferate and rapidly differentiate to PCs. Yet, transformation is restricted to LMP1$^+$/2A$^+$ GCBs that do not undergo PC-differentiation.

To allow in vivo co-expression of EBNA3A with both LMPs we generated a new *R26LMP1t2aLMP2A^{stopf}* allele that upon deletion of the stop-cassette expresses both LMPs through a 2A-self cleavage peptide (Fig. S6C). Compared to the expression from separate R26-alleles, LMP1 expression in TAT-Cre-treated *R26LMP1t2aLMP2A^{stopf}* B cells (iLMP1_2A B cells) was about 2-fold reduced, while LMP2A expression was comparable (Fig. S6D). Still, the LMP1-target FAS was induced to similar levels in iLMP1/2A and iLMP1_2A B cells, indicating robust NF-κB-activation under both conditions (Fig. S6E). iLMP1_2A B cells proliferated extensively, expressed more *Prdm1* than iLMP1 B cells and differentiated to antibody secreting CD138$^+$/B220^{low} PCs within 9 days of culture (Fig. 6F, S6F, S6G). iLMP2A cells expanded little and did not differentiate

to PCs in their lifespan (Fig. S6H-i). In contrast to iLMP1_2A B cells, iLMP1_2A/EBNA3A B cells showed blunted *Prdm1*-expression, CD138 surface staining and antibody secretion (Fig. 6F, 6G, S6F). Overexpression of *Prdm1* in iLMP1_2A/EBNA3A B cells allowed their differentiation to antibody secreting $CD138^{+}/B220^{low}$ PCs (Fig. S6J-K). Notably, the inhibition of PC-differentiation was specific to EBNA3A as retroviral transduction of EBNA1, -LP, -3B and -3C failed to inhibit differentiation of iLMP1_2A B cells (Fig. S6L). Taken together, combined expression of LMP1 and LMP2A from a single allele drives proliferation and rapid PC-differentiation of B cells, which is inhibited by EBNA3A via *Prdm1* suppression.

Transformation of LMP1 and LMP2A expressing B cells requires overexpression of EBNA3A and Myc

To test the impact of combined expression of LMP1, LMP2A and EBNA3A on B cells in vivo, we reconstituted *RAG2*^{KO}*c*γ^{KO} mice with fHSPCs from *Cd3*ε^{KO}*;Cd19-Cre; R26LMP1t2aLMP2A*^{stopf} (tpLMP1_2A mice) or *Cd3*ε^{KO}*;Cd19-Cre; R26LMP1t2aLMP2A*^{stopf}*;R26EBNA3A*^{stopf} (tpLMP1_2A/EBNA3A mice). tpLMP1_2A mice developed terminal LPD-symptoms within 30 to 60 days (Fig. 6H), with LMP1_2A expressing PCs accumulating in the spleen (Fig. S6M, S6N). Surprisingly, tpLMP1_2A/EBNA3A mice did not show an accelerated disease progression (Fig. 6H) and developed a slightly less severe splenomegaly (Fig. S6O), suggesting that EBNA3A does not promote expansion of LMP1_2A B cells. Indeed, a majority of splenocytes in tpLMP1_2A/EBNA3A mice had escaped Cre-mediated recombination of the EBNA3A-allele and expressed only LMP1_2A (Fig. 6I). This was despite EBNA3A still suppressing LMP1_2A-driven PC-differentiation in the fraction of B cells that had recombined both alleles (Fig. 6I). To determine why EBNA3A expression is counter-selected in LMP1_2A B cells we compared proliferation and survival of iLMP1_2A and iLMP1_2A/EBNA3A B cells in vitro. Both cell types expanded at similar rates (Fig. S6P). EBNA3A inhibited caspase 3 activation (Fig. S6Q) but, in stark contrast to its activity in LMP1-expressing B cells, blunted BrdU-uptake (Fig. 7A). This suggests that EBNA3A has opposing effects

on proliferation and cell survival in B cells expressing both LMPs. In vitro, inhibition of apoptosis and proliferation appear to counterbalance each other, allowing similar expansion dynamics. In vivo, the reduced proliferation might outweigh anti-apoptotic effects and cause counter-selection of EBNA3A expressing cells. EBNA3A-overexpression was previously reported to suppress proliferation of human LCLs by inhibiting *MYC* transcription (43). Similarly, we find iLMP1_2A/EBNA3A B cells to express less *Myc* mRNA and protein compared to iLMP1_2A B cells (Fig. 7B-C). In LMP1 B cells EBNA3A it did not suppress *Myc* (Fig. 7B, S5B). Retroviral overexpression of *Myc* promoted BrdU-uptake, cell cycle and cell expansion of iLMP1_2A/EBNA3A B cells, but did not elevate PC-differentiation (Fig. 7D-F, S7A-C). In iLMP1_2A B cells *Myc*-overexpression had little impact on proliferation and differentiation. To determine the impact of *Myc* activation on iLMP1_2A/EBNA3A B cell transformation, we transplanted $5x10^6$ *Myc*-transduced iLMP1_2A/EBNA3A B cells into $RAG2^{KO}c\gamma^{KO}$ mice. Within 90 days roughly one third of transplanted mice developed LMP1_2A$^+$, EBNA3A$^+$ and RV-*Myc*$^+$ lymphomas in spleen and liver (Fig. 7G, 7H). Tumors were clonal, as indicated by VDJ-diversity restriction (Fig. S7B) and expressed CD19 but not CD138 (Fig. 7H), suggesting that blocked PC-differentiation is also important in such lymphomas. $RAG2^{KO}c\gamma^{KO}$ mice transplanted with control cells, including *Myc*-transduced iLMP1_2A B cells, did not develop lymphomas within the observation period of 150 days (Fig. 7G). Thus, aberrant *Myc* activation overrides EBNA3A suppressive effects on proliferation and together with EBNA3A allows transformation of LMP1_2A B cells in vivo.

Discussion

Here we investigate interlocking functions of EBV genes during EBV-driven B cell lymphomagenesis. We had previously shown that expression of LMP1 in mouse B cells causes spontaneous LMP1-L development in T cell deficient mice (20). We now find that all LMP1-Ls aberrantly activate either *Ebf1* or *Rel* either by translocation into the Ig-locus or other unknown mechanisms, which possibly include the recurrent amplification of the *Ebf1*- and *Rel*-encoding chromosome 11. Overexpression of either gene with LMP1 in

mouse B cells efficiently facilitates their transformation in vitro and in vivo, arguing that *Ebf1* and *Rel* are potent oncogenes in LMP1-driven B cells. The finding that LMP1/EBF1-expressing B cells can grow out from single cells even suggests that this oncogene combination does not depend on additional mutations to transform at least a subset of B cells. Indeed, the frequency in which LMP1/EBF1 co-expression transforms single sorted mouse B cells in vitro (~2%) is similar to the transforming-efficiency of EBV in human B cells (~3-10%) (1, 44). Thus, co-expression of a single viral and a single somatic gene recapitulates EBV-mediated transformation of B cells in vitro and in vivo. EBF1/LMP1-driven B cell transformation is, to our knowledge, the first report of an efficient 2-factor B cell transformation, underlining the transforming potential of EBV-oncoprotein LMP1. Indeed, B cell transformation driven by *MYC*, considered to be one of the most potent oncogenes in B cells, still requires overexpression of at least two additional factors, like *BCL6/BCL2* or *BMI1/BCLXL* or *BMI1/MCL1* (27, 45). In the future mouse EBF1-LCLs might serve, like their human counterparts, as a simple and powerful tool for in vitro expansion of mature B cells, independent of exogenous cytokines or feeders.

Given their potential to transform LMP1 B cells, we considered EBF1 and c-Rel as possible surrogates for EBV proteins that would cooperate with LMP1 in EBV-driven B cell transformation. The distinct gene expression patterns of *Ebf1*^{high} and *Rel*^{high} LMP1-Ls might reflect different modes of viral lymphomagenesis. Importantly, EBF1 and to a minor extent c-REL also supported the expansion of LMP1-expressing human GCBs, indicating that the presented mouse model can predict genes that synergize with LMP1 in the transformation of human B cells.

REL is frequently amplified in human B cell lymphomas especially GCB-DLBCLs and HL, suggesting an important oncogenic role (46). Yet, no direct evidence for c-Rel oncogenicity in a mouse B cell lymphoma model has, to our knowledge, been reported. On the contrary, c-Rel was shown to be a tumor suppressor in *EμMyc* lymphomas (47). We now find *Rel* to be a potent oncogene in mouse LMP1 B cells. Aberrant *Rel*-expression likely supports LMP1-driven lymphomagenesis by promoting expression of a subset of proto-oncogenic NF-kB targets like Bcl-X and BFL-1, overcoming LMP1-mediated repression of endogenous *Rel*. Thus, transformation of mouse B cells appears

to benefit from a dual activation of NF-kB. LMP1 constitutively activates the IKK signaling cascade, while *Rel*-induction ensures sufficient expression of c-Rel-sensitive oncogenic targets.. As *REL* is not specifically overexpressed in human EBV$^+$ PT-ABC-DLBCL over EBV$^-$ cases and not commonly amplified in EBV$^+$ DLBCL cases (37, 39, 40), we suspect that other EBV gene products substitute for *REL*-overexpression during the transformation of human B cells. Possible candidates are LMP2A and viral miRNAs which have been shown to modulate LMP1-driven NF-κB signaling (48, 49). If not in PTLs, the synergy of LMP1 and c-Rel might play out in the pathogenesis of human HLs which often carry *REL*-amplifications (~20% of cases) and express LMP1$^+$ EBV latency II (~40% of cases) (50, 51). To our knowledge an analysis overlaying *REL*-amplification with LMP1-expression in HL has not yet been performed.

The recurrent activation of *Ebf1* in LMP-Ls was surprising, since *Ebf1* is not considered to be an oncogene, but has rather been described as a tumor suppressor in acute lymphoblastic leukemia (52, 53). Some cases of DLBCL were reported to carry mutated, deleted or Ig-translocated *EBF1*, but the impact of such mutations on tumorigenesis has remained elusive (38, 54–56). Interestingly, *EBF1* is among 8 genes whose knockout is lethal in human ABC-DLBCL but not GCB-DLBCL cell lines (57), supporting the idea that EBF1 plays an important role specifically in ABC-DLBCLs. We find that *Ebf1*-overexpression is sufficient to block cytokine- and LMP-driven PC-differentiation of mouse B cells. Importantly, a loss of PC-differentiation potential was previously shown to promote ABC-DLBCL onset in humans and mice (32, 58–60). As LMP1-Ls resemble ABC-DLBCLs, EBF1 likely supports transformation of LMP1 B cells through inhibition of terminal PC-differentiation.

In contrast to mouse LMP1 B cells, transformation of human B cells by EBV latency III is not known to require additional somatic mutations (1, 61). Assuming that inhibition of LMP-driven PC-differentiation is indeed a critical step in the transformation of human B cells by EBV, one would predict that EBV itself encodes an inhibitor of PC-differentiation. Indeed, the EBV-gene products LMP1, miR-BHRF1-2, EBNA1 and most recently EBNA3A and 3C were reported to impact PC-differentiation of EBV infected human B cells in vitro (62–65). We now show that EBNA3A inhibits PC-differentiation and promotes

lymphomagenesis of mouse LMP1 B cells in vivo. (EBNA3C did, for unknown reasons, not affect mouse B cells). Overexpression of *Prdm1* was sufficient to overcome EBNA3A suppressive effects on PC-differentiation in this system. Indeed, *Prdm1* is a direct target of EBNA3A in human cells (65), supporting the idea that EBNA3A engages the same pathways in mouse and human cells

As our data predicted that EBF1 can substitute for EBNA3A in LMP-driven B cell transformation, we wondered whether *EBF1* might be selectively activated in human latency II (LMPs^{+}EBNA3A^{-}) PTLs. Yet, *EBF1*-expression in human PT-ABC-DLBCL was rather reduced in latency II over latency III cases. While this was surprising, the low case number in the study might be insufficient to detect rare *EBF1*^{high} tumors. Note that in our mouse model only a subset of tumors is driven by EBF1. The low *EBF1*-expression in latency II tumors might also reflect that the progenitor cells of the such lymphomas expressed the EBV latency III program, including EBNA3 expression, as this is the default EBV-program after initial B cell infection (1). If EBNA3 expression epigenetically silences *PRDM1* at this stage as it does in human LCLs (60), this would render the malignant progeny independent of EBF1-activation, even after a switch to latency II.

Taken together, our findings indicate that shared regulation of PC-differentiation is critical for EBF1's and EBNA3A's oncogenic activity. Still, the two proteins likely have additional non-shared functions during transformation. In the case of EBNA3A one such activity might be the observed suppression of *Cdkn2a* and *Bcl2l11*. Although knockout of either gene was insufficient to promote the expansion of LMP1 B cells, their coregulation might still serve this purpose, an issue that remains to be addressed.

Co-expression of LMP1 and LMP2A, as observed in the EBV growth program, promoted B cell expansion and PC-differentiation, but transformation was still restricted to cells that did not undergo PC-differentiation. Although EBNA3A suppressed differentiation and supported survival of LMP1/2A expressing B cells, it did not promote their transformation, but blunted their proliferation through the inhibition of *Myc* transcription. This is in line with reports that EBNA3A overexpression inhibits proliferation of human LCLs by silencing

EBNA2-driven *MYC*-transcription (43), likely through the binding EBNA3A to multiple *MYC*-enhancer sites (66). As one would then predict, overexpression of *Myc* in LMP1_2A/EBNA3A mouse B cells mitigated the repressive effects of EBNA3A and allowed their transformation to lymphomas in vivo. This dependence on *Myc*-activation strikingly resembles the dependence of EBV-driven B cell transformation on the *MYC*-activator EBNA2 (67). Importantly, transplantation of LMP1, LMP2A, EBNA3A and MYC co-expressing B cells caused clonal lymphomagenesis, arguing that transformation of such cells still depends on secondary events. Defining such secondary events along the lines of the present analysis might shed light on additional functions of other EBV genes during the transformation of human B cells. Unexpectedly, EBNA3A did not impact *Myc* transcription in LMP1-only B cells. This might be due to elevated expression of LMP1 from the *R26LMP1* over the *R26LMP1t2aLMP2A* allele. More likely, and consistent with the highly cell type-, signaling- and EBV-dependent selection of *Myc*-enhancers (68–72), integrated LMP1 and LMP2A signaling engages *Myc*-enhancers distinct from those used in LMP1-only B cells and more sensitive to EBNA3A. Such differential use of *MYC*-enhancers should be addressed in future studies, albeit in human B cells.

In summary, our conditional EBV-transgenic mice represent a novel system to study interlocking functions of viral oncogenes in B cell lymphomagenesis. The presented data reveal a model of EBV-driven B cell lymphomagenesis in which LMPs induce B cell proliferation but also promote differentiation to non-transforming PCs. EBNA3A blocks PC-differentiation but simultaneously inhibits MYC-driven proliferation. This inhibition does not play out in the presence of the EBV *MYC*-activator EBNA2, allowing B cell transformation.

Methods

Mouse strains and handling

Cd19cre (73), *Cγ1-Cre* (74), *Rosa26LMP1*^{stopf} (21), *Rosa26LMP2A*^{stopf} (41), *Rosa26CAS9*^{tg} (75), *Rag2*^{KO} (76), *IL2Rcγ*^{KO} (*cγ*^{KO}) (77) and *Cd3ε*^{KO} (78) mouse strains

were described before. Unless noted, mice were used between 8 and 30 weeks of age and indiscriminately of their sex. Cre- and R26-alleles were always used heterozygous. Animals developing pathologies did not succumb to the disease but were sacrificed once defined humane termination criteria were reached. Animal procedures were approved by the Landesamt für Gesundheit und Soziales Berlin (G0049/15, G0374/13 and G0135/11).

Data presentation and statistical analysis

Unless noted otherwise, single dots or indicated n-values represent number of biological replicates from independent mice or human donors. Unless noted otherwise, bars represent mean ± SD. Two-sided tests for significance were chosen by assumed data distribution and variation and are noted in the figure legends. When noted p-values were adjusted for multiple testing.

Data availability

RNA-sequencing, exome sequencing and array CHG data are available at the GEO repository under the accession number GSE136075 (Preliminary token for reviewers: gnwdgaomnzshfir).

Further methods and critical reagents can be found in the SI-Appendix.

Acknowledgement

We thank all members of the Rajewsky laboratory for assistance and discussion. We thank the Genomics-, Transgenics- and Flow cytometry-core facilities at the MDC as well as F. Lasitschka, R. Rad and N. Gross for technical assistance. We thank M. Janz, W. Hammerschmidt, E. Kieff, B. Gewurz and B. Zhao for sharing materials. This work was

supported by the European Research Council Advanced Grant No. 268921 to K.R. and by the „Helmholtz Alliance Preclinical Comprehensive Cancer Center“ of the Helmholtz Association‘s Initiative and Networking Fund (HA-305) and by the Helmholtz-Gemeinschaft, Zukunftsthema "Immunology and Inflammation" (ZT-0027). R.C. and D.H. were supported by The Medical Research Council, UK.

References

1. L. S. Young, L. F. Yap, P. G. Murray, Epstein–Barr virus: more than 50 years old and still providing surprises. *Nat. Rev. Cancer* **16**, 789–802 (2016).
2. G. S. Taylor, H. M. Long, J. M. Brooks, A. B. Rickinson, A. D. Hislop, The Immunology of Epstein-Barr Virus–Induced Disease. *Annu. Rev. Immunol.* **33**, 787–821 (2015).
3. S. H. Swerdlow, S. A. Webber, A. Chadburn, J. A. Ferry., “Post-transplant lymphoproliferative disorders” in *WHO Classification of Tumours of Haematopoietic and Lymphoid Tissues*, 4th Ed., (International Agency for Research on Cancer, 2008), pp. 343–349.
4. J. Morscio, T. Tousseyn, Recent insights in the pathogenesis of post-transplantation lymphoproliferative disorders. *World J. Transplant.* **6**, 505–16 (2016).
5. A. Kieser, K. R. Sterz, “The Latent Membrane Protein 1 (LMP1)” in *Current Topics in Microbiology and Immunology*, (2015), pp. 119–149.
6. J. Rastelli, *et al.*, LMP1 signaling can replace CD40 signaling in B cells in vivo and has unique features of inducing class-switch recombination to IgG1. *Blood* **111**, 1448–55 (2008).
7. O. Cen, R. Longnecker, “Latent Membrane Protein 2 (LMP2)” in *Current Topics in Microbiology and Immunology*, (2015), pp. 151–180.
8. R. R. G. Caldwell, J. J. B. Wilson, S. J. Anderson, R. Longnecker, Epstein-Barr virus LMP2A drives B cell development and survival in the absence of normal B cell receptor signals. *Immunity* **9**, 405–411 (1998).
9. S. Casola, *et al.*, B cell receptor signal strength determines B cell fate. *Nat. Immunol.* **5**, 317–327 (2004).
10. B. Kempkes, P. D. Ling, “EBNA2 and Its Coactivator EBNA-LP” in *Current Topics in Microbiology and Immunology*, (2015), pp. 35–59.
11. M. J. Allday, Q. Bazot, R. E. White, “The EBNA3 Family: Two Oncoproteins and a Tumour Suppressor that Are Central to the Biology of EBV in B Cells” in *Current Topics in Microbiology and Immunology*, (2015), pp. 61–117.
12. F. Wang, Nonhuman primate models for Epstein-Barr virus infection. *Curr. Opin. Virol.* **3**, 233–7 (2013).

13. J. Törnell, *et al.*, Expression of Epstein-Barr nuclear antigen 2 in kidney tubule cells induce tumors in transgenic mice. *Oncogene* **12**, 1521–8 (1996).

14. D. S. Huen, A. Fox, P. Kumar, P. F. Searle, Dilated heart failure in transgenic mice expressing the Epstein-Barr virus nuclear antigen-leader protein. *J. Gen. Virol.* **74 (Pt 7)**, 1381–91 (1993).

15. R. G. Caldwell, R. C. Brown, R. Longnecker, Epstein-Barr virus LMP2A-induced B-cell survival in two unique classes of EmuLMP2A transgenic mice. *J. Virol.* **74**, 1101–13 (2000).

16. M.-S. Kang, *et al.*, Epstein-Barr virus nuclear antigen 1 does not induce lymphoma in transgenic FVB mice. *Proc. Natl. Acad. Sci.* **102**, 820–825 (2005).

17. J. B. Wilson, J. L. Bell, A. J. Levine, Expression of Epstein-Barr virus nuclear antigen-1 induces B cell neoplasia in transgenic mice. *EMBO J.* **15**, 3117–26 (1996).

18. W. Kulwichit, *et al.*, Expression of the Epstein–Barr virus latent membrane protein 1 induces B cell lymphoma in transgenic mice. *Proc. Natl. Acad. Sci.* **95**, 11963 (1998).

19. C. Münz, Humanized mouse models for Epstein Barr virus infection. *Curr. Opin. Virol.* **25**, 113–118 (2017).

20. B. Zhang, *et al.*, Immune Surveillance and Therapy of Lymphomas Driven by Epstein-Barr Virus Protein LMP1 in a Mouse Model. *Cell* **148**, 739–751 (2012).

21. T. Yasuda, *et al.*, Studying Epstein-Barr Virus Pathologies and Immune Surveillance by Reconstructing EBV Infection in Mice. *Cold Spring Harb. Symp. Quant. Biol.* **78**, 259–263 (2013).

22. C. P. Hans, *et al.*, Confirmation of the molecular classification of diffuse large B-cell lymphoma by immunohistochemistry using a tissue microarray. *Blood* **103**, 275–282 (2004).

23. J. C. Strefford, Q. An, C. J. Harrison, Cell Cycle Modeling the molecular consequences of unbalanced translocations in cancer: Lessons from acute lymphoblastic leukemia. *Cell Cycle* **8**, 2175–2184 (2009).

24. R. Küppers, Mechanisms of B-cell lymphoma pathogenesis. *Nat. Rev. Cancer* **5**, 251–262 (2005).

25. J. M. Wroblewski, A. Copple, L. P. Batson, C. D. Landers, J. R. Yannelli, Cell surface phenotyping and cytokine production of Epstein-Barr Virus (EBV)-transformed lymphoblastoid cell lines (LCLs). *J. Immunol. Methods* **264**, 19–28 (2002).

26. E. D. Cahir-McFarland, *et al.*, Role of NF-kappa B in cell survival and transcription of latent membrane protein 1-expressing or Epstein-Barr virus latency III-infected cells. *J. Virol.* **78**, 4108 (2004).

27. R. Caeser, *et al.*, Genetic modification of primary human B cells to model high-grade lymphoma. *Nat. Commun.* **10**, 4543 (2019).

28. R. Nechanitzky, *et al.*, Transcription factor EBF1 is essential for the maintenance of B cell identity and prevention of alternative fates in committed cells. *Nat. Immunol.* **14**, 867–875 (2013).

29. W. Shi, *et al.*, Transcriptional profiling of mouse B cell terminal differentiation defines a signature for antibody-secreting plasma cells. *Nat. Immunol.* **16**, 663–673 (2015).

30. T. Nojima, *et al.*, In-vitro derived germinal centre B cells differentially generate memory B or plasma cells in vivo. *Nat. Commun.* **2**, 465 (2011).

31. K. Roy, *et al.*, A Regulatory Circuit Controlling the Dynamics of NFκB cRel Transitions B Cells from Proliferation to Plasma Cell Differentiation. *Immunity* **50**, 616-628.e6 (2019).

32. D. P. Calado, *et al.*, Constitutive Canonical NF-κB Activation Cooperates with Disruption of BLIMP1 in the Pathogenesis of Activated B Cell-like Diffuse Large Cell Lymphoma. *Cancer Cell* **18**, 580–589 (2010).

33. M. Swanson-Mungerson, R. Bultema, R. Longnecker, Epstein-Barr Virus LMP2A Enhances B-Cell Responses In Vivo and In Vitro. *J. Virol.* **80**, 6764–70 (2006).

34. J. Morscio, *et al.*, Gene expression profiling reveals clear differences between EBV-positive and EBV-negative posttransplant lymphoproliferative disorders. *Am. J. Transplant.* **13**, 1305–1316 (2013).

35. E. Vakiani, *et al.*, Genetic and phenotypic analysis of B-cell post-transplant lymphoproliferative disorders provides insights into disease biology. *Hematol. Oncol.* **26**, 199–211 (2008).

36. F. E. Craig, *et al.*, Gene expression profiling of epstein-barr virus-positive and -negative monomorphic B-cell posttransplant lymphoproliferative disorders. *Diagnostic Mol. Pathol.* **16**, 158–168 (2007).

37. J. Finalet Ferreiro, *et al.*, EBV-Positive and EBV-Negative Posttransplant Diffuse Large B Cell Lymphomas Have Distinct Genomic and Transcriptomic Features. *Am. J. Transplant.* **16**, 414–425 (2016).

38. T. Menter, *et al.*, Mutational landscape of B-cell post-transplant lymphoproliferative disorders. *Br. J. Haematol.* **178**, 48–56 (2017).

39. A. Rinaldi, *et al.*, Single nucleotide polymorphism-arrays provide new insights in the pathogenesis of post-transplant diffuse large B-cell lymphoma. *Br. J. Haematol.* **149**, 569–577 (2010).

40. H. A. Poirel, *et al.*, Characteristic pattern of chromosomal imbalances in posttransplantation lymphoproliferative disorders: Correlation with histopathological subcategories and EBV status. *Transplantation* **80**, 176–184 (2005).

41. T. Wirtz, *et al.*, Mouse model for acute Epstein-Barr virus infection. *Proc. Natl. Acad. Sci. U. S. A.* **113**, 13821–13826 (2016).

42. T. Minamitani, *et al.*, Mouse model of Epstein-Barr virus LMP1- and LMP2A-driven germinal center B-cell lymphoproliferative disease. *Proc. Natl. Acad. Sci. U. S. A.* **114**, 4751–4756 (2017).

43. A. Cooper, *et al.*, EBNA3A association with RBP-Jkappa down-regulates c-myc and Epstein-Barr virus-transformed lymphoblast growth. *J. Virol.* **77**, 999–1010 (2003).

44. C. Shannon-Lowe, *et al.*, Epstein-Barr virus-induced B-cell transformation: Quantitating events from virus binding to cell outgrowth. *J. Gen. Virol.* **86**, 3009–3019 (2005).

45. K. Högstrand, A. Grandien, MYC-driven malignant transformation of mature murine B cells requires inhibition of both intrinsic apoptosis and p53 activity. *Eur. J. Immunol.* **49**, 375–385 (2019).

46. J. E. Hunter, J. Leslie, N. D. Perkins, c-Rel and its many roles in cancer: an old story with

new twists. *Br. J. Cancer* **114**, 1–6 (2016).

47. J. E. Hunter, *et al.*, The NF-κB subunit c-Rel regulates Bach2 tumour suppressor expression in B-cell lymphoma. *Oncogene* **35**, 3476–3484 (2016).

48. Y. Chen, D. Fachko, N. S. Ivanov, C. M. Skinner, R. L. Skalsky, Epstein-Barr virus microRNAs regulate B cell receptor signal transduction and lytic reactivation. *PLoS Pathog.* **15** (2019).

49. L. Guasparri, D. Bubman, E. Cesarman, EBV LMP2A affects LMP1-mediated NF-{kappa}B signaling and survival of lymphoma cells by regulating TRAF2 expression. *Blood* **111**, 3813–3820 (2008).

50. J. I. Martín-Subero, *et al.*, Recurrent involvement of the REL and BCL11A loci in classical Hodgkin lymphoma. *Blood* **99**, 1474–7 (2002).

51. R. Küppers, A. Engert, M.-L. Hansmann, Hodgkin lymphoma. *J. Clin. Invest.* **122**, 3439–47 (2012).

52. C. G. Mullighan, *et al.*, Genome-wide analysis of genetic alterations in acute lymphoblastic leukaemia. *Nature* **446**, 758–764 (2007).

53. E. Tijchon, J. Havinga, F. N. van Leeuwen, B. Scheijen, B-lineage transcription factors and cooperating gene lesions required for leukemia development. *Leukemia* **27**, 541–552 (2013).

54. H. Bouamar, *et al.*, A capture-sequencing strategy identifies IRF8, EBF1, and APRIL as novel IGH fusion partners in B-cell lymphoma. *Blood* **122**, 726–33 (2013).

55. K. Karube, *et al.*, Integrating genomic alterations in diffuse large B-cell lymphoma identifies new relevant pathways and potential therapeutic targets. *Leukemia* **32**, 675–684 (2018).

56. R. Schmitz, *et al.*, Genetics and Pathogenesis of Diffuse Large B-Cell Lymphoma. *N. Engl. J. Med.* **378**, 1396–1407 (2018).

57. A. Reddy, *et al.*, Genetic and Functional Drivers of Diffuse Large B Cell Lymphoma. *Cell* **171**, 481-494.e15 (2017).

58. W. Tam, *et al.*, Mutational analysis of PRDM1 indicates a tumor-suppressor role in diffuse large B-cell lymphomas. *Blood* **107**, 4090–4100 (2006).

59. L. Pasqualucci, *et al.*, Inactivation of the PRDM1/BLIMP1 gene in diffuse large B cell lymphoma. *J. Exp. Med.* **203**, 311–317 (2006).

60. J. Mandelbaum, *et al.*, BLIMP1 is a tumor suppressor gene frequently disrupted in activated B cell-like diffuse large B cell lymphoma. *Cancer Cell* **18**, 568–79 (2010).

61. R. Küppers, B cells under influence: transformation of B cells by Epstein–Barr virus. *Nat. Rev. Immunol.* **3**, 801–812 (2003).

62. A. Onnis, *et al.*, Epstein-Barr nuclear antigen 1 induces expression of the cellular microRNA hsa-miR-127 and impairing B-cell differentiation in EBV-infected memory B cells. New insights into the pathogenesis of Burkitt lymphoma. *Blood Cancer J.* **2**, e84 (2012).

63. J. Ma, *et al.*, EBV-miR-BHRF1-2 targets PRDM1/Blimp1: potential role in EBV lymphomagenesis. *Leukemia* **30**, 594–604 (2016).

64. K. Vrzalikova, *et al.*, Down-regulation of BLIMP1α by the EBV oncogene, LMP-1, disrupts the plasma cell differentiation program and prevents viral replication in B cells: implications

for the pathogenesis of EBV-associated B-cell lymphomas. *Blood* **117**, 5907–17 (2011).

65. C. T. Styles, *et al.*, EBV epigenetically suppresses the B cell-to-plasma cell differentiation pathway while establishing long-term latency. *PLoS Biol.* **15**, e2001992 (2017).

66. S. C. S. Schmidt, *et al.*, Epstein-Barr virus nuclear antigen 3A partially coincides with EBNA3C genome-wide and is tethered to DNA through BATF complexes. *Proc. Natl. Acad. Sci. U. S. A.* **112**, 554–9 (2015).

67. J. I. I. Cohen, F. Wang, J. Mannick, E. Kieff, Epstein-Barr virus nuclear protein 2 is a key determinant of lymphocyte transformation. *Proc. Natl. Acad. Sci.* **86**, 9558 (1989).

68. J. Schuijers, *et al.*, Transcriptional Dysregulation of MYC Reveals Common Enhancer-Docking Mechanism. *Cell Rep.* **23**, 349–360 (2018).

69. C. Bahr, *et al.*, A Myc enhancer cluster regulates normal and leukaemic haematopoietic stem cell hierarchies. *Nature* **553**, 515–520 (2018).

70. D. Herranz, *et al.*, A NOTCH1-driven MYC enhancer promotes T cell development, transformation and acute lymphoblastic leukemia. *Nat. Med.* **20**, 1130–1137 (2014).

71. S. Jiang, *et al.*, The Epstein-Barr Virus Regulome in Lymphoblastoid Cells. *Cell Host Microbe* **22**, 561-573.e4 (2017).

72. H. Zhou, *et al.*, Epstein-Barr Virus Oncoprotein Super-enhancers Control B Cell Growth. *Cell Host Microbe* **17**, 205–216 (2015).

73. R. C. Rickert, J. Roes, K. Rajewsky, B lymphocyte-specific, Cre-mediated mutagenesis in mice. *Nucleic Acids Res.* **25**, 1317–8 (1997).

74. S. Casola, *et al.*, Tracking germinal center B cells expressing germ-line immunoglobulin 1 transcripts by conditional gene targeting. *Proc. Natl. Acad. Sci.* **103**, 7396–7401 (2006).

75. V. T. Chu, *et al.*, Efficient generation of Rosa26 knock-in mice using CRISPR/Cas9 in C57BL/6 zygotes. *BMC Biotechnol.* **16**, 4 (2016).

76. Z. Hao, K. Rajewsky, Homeostasis of Peripheral B Cells in the Absence of B Cell Influx from the Bone Marrow. *J. Exp. Med.* **194**, 1151–1164 (2001).

77. J. P. DiSanto, W. Müller, D. Guy-Grand, A. Fischer, K. Rajewsky, Lymphoid development in mice with a targeted deletion of the interleukin 2 receptor gamma chain. *Proc. Natl. Acad. Sci. U. S. A.* **92**, 377–81 (1995).

78. M. Malissen, *et al.*, Altered T cell development in mice with a targeted mutation of the CD3-epsilon gene. *Embo J* **14**, 4641–53 (1995).

Figure legends

Fig. 1. *Ebf1* and *Rel* are aberrantly activated in LMP1-Lymphoma

A Experimental overview LMP1-lymphoma (LMP1-L) cohort (B-F) **B** Survival curve **C** Representative M-FISH of (11;12)-translocations in LMP1-CLs 37 and 43 **D** Translocations in sorted (huCD2$^+$) 2^{ry}LMP1-Ls as determined by exome- and sanger-sequencing (LMP1-L 31 and 43) or as suggested by CNVs in array-CGH (LMP1-L 37). Arrows indicate open reading frame orientation **E,F** RNA sequencing of sorted splenic B cells (CD19$^+$CD38$^-$), tpLMP1 B cells (day 18-20 post transplantation (p.t), huCD2$^+$) and 2^{ry}LMP1-Ls (huCD2$^+$) **E** Heatmap showing FPKM-normalized expression **F** Principle component analysis on the 500 most variable genes

Fig. 2. *Ebf1*- or *Rel*-overexpression supports transformation of LMP1 B cells

A Experimental overview (a-g) **B** Growth curve of transduced (GFP$^+$) cells **C** Quantification of outgrowing single sorted transduced (GFP$^+$) cells on MEF-feeder. Bars represent median outgrowth-frequency. Number of biological replicates showing any outgrowth is indicated. Images show representative wells on day 21 post TAT-cre **D** Survival curve of transplanted *RAG2*^{KO}*c*γ^{KO} mice. **E-G** Analysis of *RAG2*^{KO}*c*γ^{KO} mice transplanted with 3*10^5 GFP$^+$ cells. Analysis was performed at symptom onset or between day 11 and 22 (control groups). **E** Representative organ-images day 11 (RV-GFP/RV-*Ebf1*) day 21 (RV-LMP1) **F** FACS-analysis of splenocytes from (E) **G** Cell count of GFP$^+$/huCD2$^+$ cells in indicated organs. n=2 (αCD40/IL-4 treated groups) n=4 (iLMP1 RV-GFP); n=5 (iLMP1 RV-*Ebf1* or iLMP1 RV-*Rel*) **H** Human tonsillar GCBs were cultured on CD40-L/IL-21 feeder cells and transduced with RVs encoding GFP, LMP1-ires-GFP, *Ebf1*-ires-mCherry or *Rel*-ires-mCherry. Starting day 5 cells were cultured on feeders without CD40-L/IL-21. Fold change of reporter$^+$ cell number on day 12 over day 5 is presented (n=15; n=12 (LMP1/RV-*Rel* and RV-*Rel*)). All data are presented as mean ±

SD. Significance was calculated by Welch's t-test (G) or one sample t-test (H) (*p<0.05;**p<0.005;***p<0.0005)

Fig. 3. Ebf1 inhibits PC-differentiation of LMP1 B cells

A-D Further analysis of 2^{ry}LMP1-Ls from Fig. 1 **A** Heatmap showing FPKM-normalized expression of B cell and PC transcription factors (TF) in RNA-sequencing **B** FACS-analysis of splenocytes from tpLMP1 mice before lymphomagenesis (day 30 post-transplant) **C** FACS-analysis of a representative splenic *Ebf1*^{high} 2^{ry}LMP1-L **D** Quantification of CD138 expression on huCD2$^+$ cells in (B) and (C). Bars indicate median. n=3 (tpLMP1 and Ebf1^{high} LMP1-L), n=9 (*Rel*^{high} LMP1-L) **E,F** RNA-sequencing of iLMP1 B cells transduced on day 1 with RVs encoding GFP, *Ebf1*-ires-GFP or *Rel*-ires-GFP. RNA was isolated from FACS-sorted (GFP$^+$/huCD2$^+$) cells on day 6 post TAT-Cre. Naive splenic B cells (CD19$^+$/CD38$^+$) from wildtype mice are presented as a control **E** Heatmap showing FPKM-normalized expression **F** Gene set enrichment analysis of a gene set differentially expressed in splenic PCs over GCBs (29) run in the space of genes differentially expressed between GFP- and *Ebf1*-transduced iLMP1 B cells on day 6.

Fig. 4. EBNA3A inhibits PC-differentiation

A iLMP1 B cells were transduced with RVs encoding mCherry or indicated EBNAs (reported by ires-mCherry). FACS-based quantification of mCherry$^+$ cells day 7 over day 4 is presented (n=5) **B-F** Analysis of *Cd19-cre;R26EBNA3A*^{stopf} and *Cd19-cre;R26BFP*^{stopf} mice **B** Representative FACS-analysis of spleens **C** Survival curve **D** Quantification of BFP expression in bone marrow pro- (CD93$^+$B220$^+$IgM$^-$IgD$^-$CD19$^+$c-kit$^{+/low}$), pre- (CD93$^+$B220$^+$IgM$^-$IgD$^-$CD19$^+$c-kit$^-$), immature- (CD93$^+$B220$^+$IgM$^+$IgD$^-$) and splenic mature- (CD93$^-$B220$^+$CD19$^+$IgM$^+$IgD$^+$) B cells. n=9 (*Cd19-Cre;BFP*^{stopf}) n=10 (*Cd19-Cre;EBNA3A*^{stopf}) **E** Representative FACS-analysis and quantification of BFP expression in bone marrow (CD138$^+$CD267$^+$) PCs; n=12 (*Cd19-Cre;BFP*^{stopf}) n=14 (*Cd19-Cre;EBNA3A*^{stopf}) **F** Elispot for total ASCs in sorted BFP$^+$ bone marrow cells; n=6. Images show representative wells with 4*10^4 cells. All data are presented as mean ± SD.

Significance was calculated using a one-way Anova with P-value adjusted via Dunnett (A), two-way Anova with Sidak's multiple comparisons test (D), Mann-Whitney U test (E), Welch's t-test (F) (*p<0.05;**p<0.005;***p<0.0005;n.s. non-significant)

Fig. 5. EBNA3A inhibits PC-differentiation and supports expansion of LMP1 B cells

A-D iBFP, iEBNA3A, iLMP1 and iLMP1/EBNA3A B cells **A** Growth curve of bulk cultured cells. n=4, n=5 (iLMP1) **B** FACS-based quantification of BrdU-uptake on day 6 post TAT-Cre. n=6 **C** FACS-based quantification of active-caspase 3 on day 6 post TAT-Cre. n=10 **D** Heatmap showing FPKM-normalized gene expression in RNA-sequencing performed on sorted hucd2+ (iLMP1) or huCD2^{+}BFP^{+} (iLMP1/EBNA3A) cells day 6 post TAT-Cre. Splenic naïve (CD19^{+}CD38^{-}) B cells (from Fig. 3E) serve as a control **E-H** *RAG2^{KO}cγ^{KO}* mice were reconstituted with fHSPCs from *Cd3ε^{KO};Cd19-Cre;R26LMP1^{stopf}* (tpLMP1) or *Cd3ε^{KO};Cd19-Cre;R26LMP1$^{stopf/}$EBNA3A^{stopf}* (tpLMP1/EBNA3A) mice. **E** Survival curve **F** Representative image of spleens and quantification of splenic weight at symptom onset (tpLMP1/EBNA3A) or day 32-41 p.t. (tpLMP1); n=3 (*RAG2^{KO}cγ^{KO}*), n=6 (tpLMP1), n=10 (tpLMP1/EBNA3A) **G** Immuno-histology on splenic sections day 36 p.t. (representative for 3 independent mice per group). Splenic section of a *RAG2^{KO}cγ^{KO}* mouse is presented as negative control **H** Elispot for total ASCs in sorted reporter^{+} splenic cells at symptom onset or day 32-41 p.t. (tpLMP1). Quantification was normalized to mean ASC-frequency in tpLMP1 conditions. Images show representative wells with 1.5*10^{5} cells. n=6 (tpLMP1), n=4 (tpLMP1/EBNA3A). All data are presented as mean ± SD. Significance was calculated using a student's t-test (A,B,C,F) or Welch's t-test (H) (*p<0.05; **p<0.005; ***p< 0.0005)

Fig. 6. EBNA3A blocks PC-differentiation of LMP1 and LMP2A B cells.

A Experimental overview (B-D) **B** Representative FACS-analysis of spleens from donor animals and recipient animals at 7-28 days p.t (quantification in Fig. S6A). **C** Survival curve **D** Representative images of LMP1/2A^{+} lymphomas arising in (C) **E** Representative FACS-analysis and quantification of CD19/CD138 expression on huCD2^{+}GFP^{+} cells in lymphomas arising in (C); n=3 **F,G** iLMP1, iLMP1_2A and iLMP1_2A/EBNA3A B cells analyzed day 9 post TAT-Cre **F** FACS-based quantification of CD138^{+}/B220^{low} PCs ; n=3 (iLMP1), n=11 (iLMP1_2A), n=9 (iLMP1_2A/EBNA3A) **G** Elispot for total ASCs among sorted reporter^{+} cells. Images show representative wells with 120 cells; n=9 **H,I** RAG2^{KO}cγ^{KO} mice were reconstituted with fHSPCs from *Cd3ε^{KO};Cd19-Cre R26LMP1_LMP2A^{stopf}* (tpLMP1_2A) or *Cd3ε^{KO};Cd19-Cre R26LMP1_LMP2A^{stopf};EBNA3A^{stopf}* (tpLMP1_2A/EBNA3A) mice. **H** Survival curve **I** Representative FACS-analysis of splenocytes from tpLMP1_2A/EBNA3A mice at symptom onset. Quantifications shows expression of LMP1_2A (huCD2^{+}) and EBNA3A (BFP^{+}) in whole splenocytes or CD19/CD138 expression on indicated populations. n=7. All data are presented as mean ± SD. Significance was calculated using a Mann-Whitney U test (G,I), or one-way Anova with p-value adjusted via Dunnett (F) (*p<0.05;**p<0.005;***p< 0.0005)

Fig. 7. Transformation of LMP1_2A B cells requires overexpression of EBNA3A and Myc

A-H Analysis of iEBNA3A, iLMP1, iLMP1_2A and iLMP1_2A/EBNA3A B cells **A** Representative FACS-analysis and quantification of BrdU-incorporation day 6 post TAT-Cre; n=7 (iLMP1_2A), n=6 (iLMP1_2A/EBNA3A) **B** RT-qPCR-based quantification of *Myc*-expression day 6 post TAT-Cre; n=17 (iLMP1), n=14 (iLMP1/EBNA3A), n=11 (iLMP1_2A and iLMP1_2A/EBNA3A) **C** Western blot of total cell lysates day 6 post TAT-Cre. Myc^{high} LMP1^{-} LMP2A^{-} mouse cell line 19pp serves as expression-control **D**

Experimental overview (E-H). iEBNA3A cells were stimulated with αCD40 (2μg/ml) and IL-4 (20ng/ml) to allow transduction. **E** Growth curve of transduced (GFP^+ or $mCherry^+$) cells in bulk **F** Representative FACS-analysis and quantification of BrdU-uptake on day 6 post TAT-Cre; n=6 **G-H** Analysis of *RAG2*^{KO}*c*γ^{KO} mice transplanted with transduced cells of 3 independent donors per group **G** Survival curve **H** Representative organ images and FACS-analysis of mice transplanted with RV-*Myc* transduced iLMP1_2A/EBNA3A B cells at disease onset. Quantifications show BFP/mCherry-expression in $huCD2^+$ cells and CD19/CD138-expression on $huCD2^+/BFP^+/mCherry^+$ cells. n=3. All data are presented as mean ± SD. Significance was calculated using a student's t-test (A), Man-Whitney U test (B), or paired student's t test (E,F) (*p<0.05;**p<0.005;***p<0.0005;n.s. non-significant)

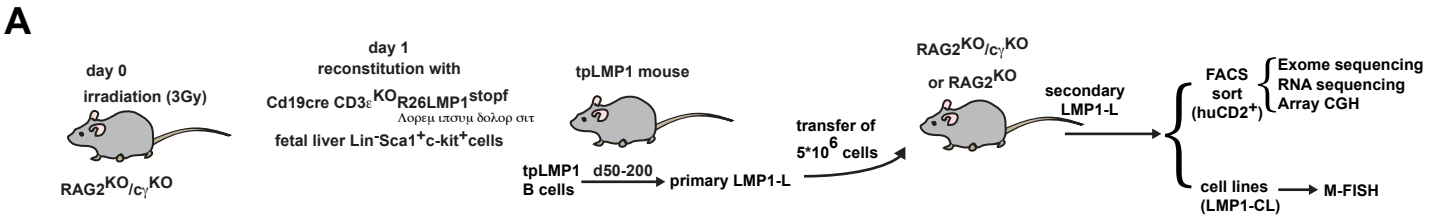
A
day 0
irradiation (3Gy)
RAG2KO/cγKO
day 1
reconstitution with
Cd19cre CD3εKOR26LMP1stopf
Λορεμ ιπσυμ δολορ σιτ
fetal liver Lin-Sca1+c-kit+cells
tpLMP1 mouse
tpLMP1 B cells
d50-200
primary LMP1-L
transfer of 5*10^6 cells
RAG2KO/cγKO or RAG2KO
secondary LMP1-L
FACS sort (huCD2+)
Exome sequencing
RNA sequencing
Array CGH
cell lines (LMP1-CL)
M-FISH

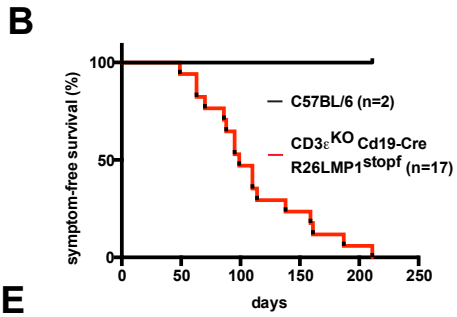
B
symptom-free survival (%)
100
50
0
0
50
100
150
200
250
days
C57BL/6 (n=2)
CD3εKO Cd19-Cre
R26LMP1stopf (n=17)

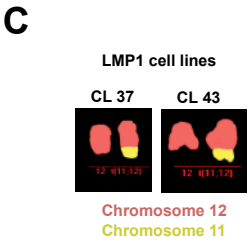
C
LMP1 cell lines
CL 37
CL 43
Chromosome 12
Chromosome 11

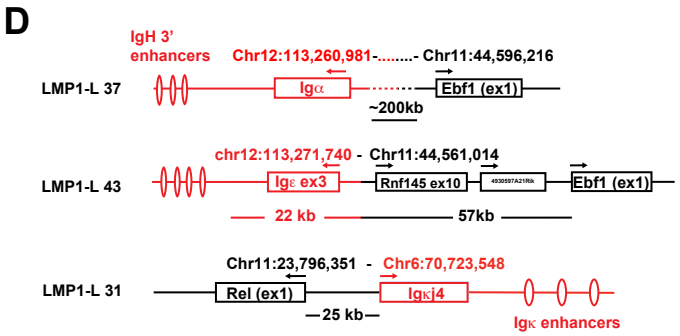
D
IgH 3' enhancers
Chr12:113,260,981-.....- Chr11:44,596,216
LMP1-L 37
Igα
Ebf1 (ex1)
~200kb
chr12:113,271,740 - Chr11:44,561,014
LMP1-L 43
Igε ex3
Rnf145 ex10
Ebf1 (ex1)
22 kb
57kb
Chr11:23,796,351 - Chr6:70,723,548
LMP1-L 31
Rel (ex1)
Igκj4
25 kb
Igκ enhancers

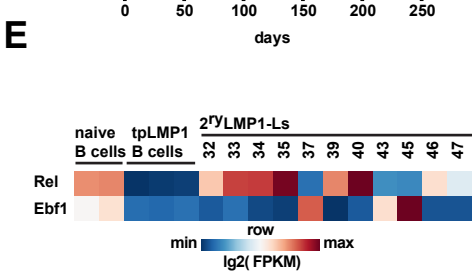
E
naive B cells
tpLMP1 B cells
2ryLMP1-Ls
32
33
34
35
37
39
40
43
45
46
47
Rel
Ebf1
row
min
max
lg2(FPKM)

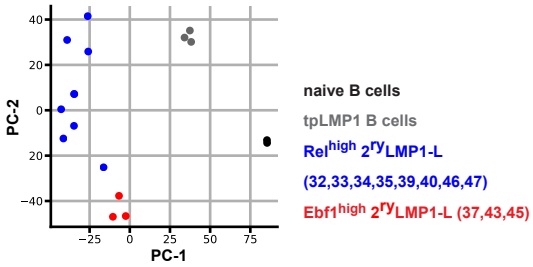
F
PC-2
PC-1
40
20
0
20
−40
−25
0
25
50
75
naive B cells
tpLMP1 B cells
Relhigh 2ryLMP1-L
(32,33,34,35,39,40,46,47)
Ebf1high 2ryLMP1-L (37,43,45)

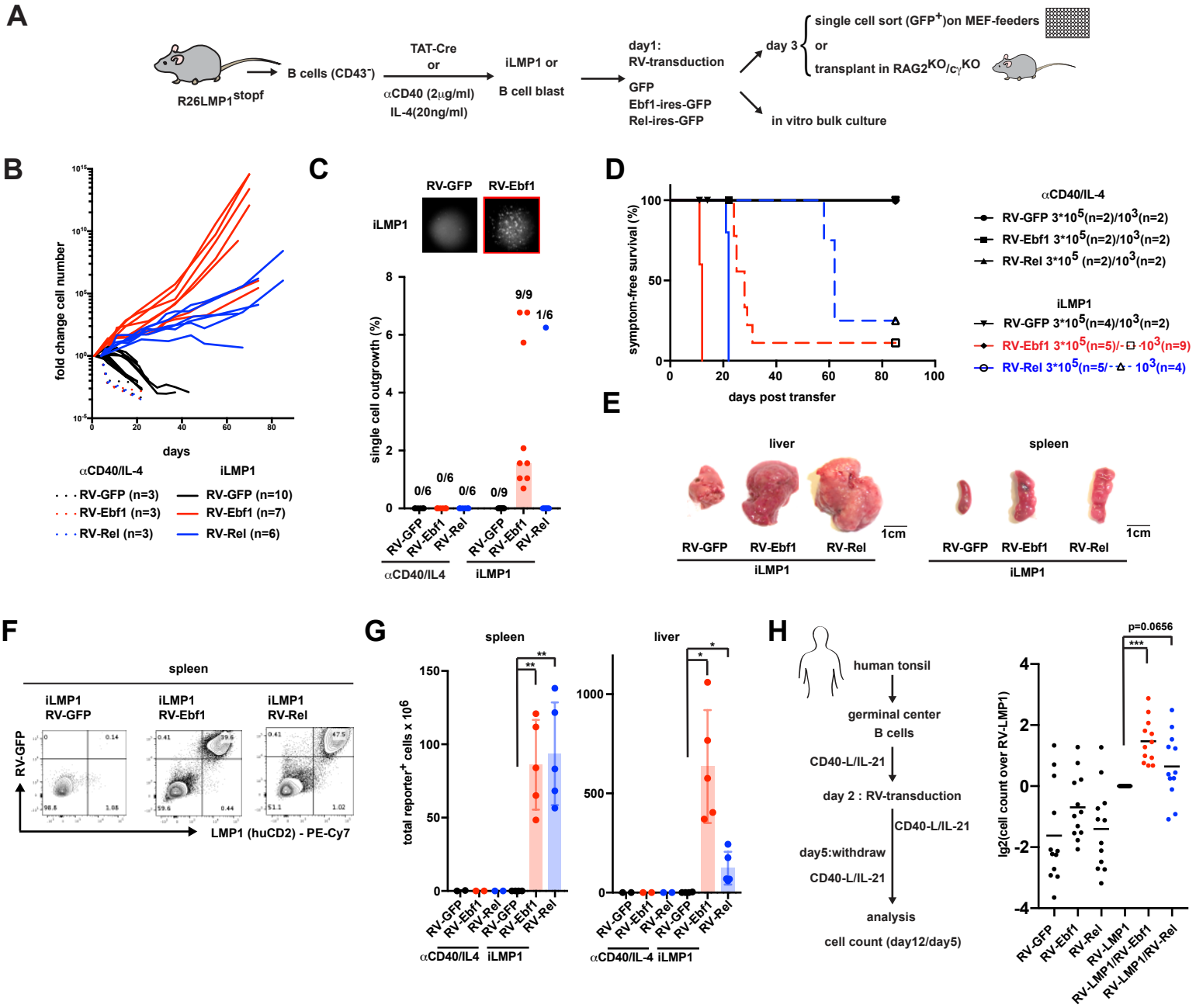
A
R26LMP1stopf
B cells (CD43-)
TAT-Cre
or
αCD40 (2μg/ml)
IL-4(20ng/ml)
iLMP1 or
B cell blast
day1:
RV-transduction
GFP
Ebf1-ires-GFP
Rel-ires-GFP
day 3
single cell sort (GFP+)on MEF-feeders
or
transplant in RAG2KO/cγKO
in vitro bulk culture
B
fold change cell number
days
αCD40/IL-4
iLMP1
RV-GFP (n=3)
RV-Ebf1 (n=3)
RV-Rel (n=3)
RV-GFP (n=10)
RV-Ebf1 (n=7)
RV-Rel (n=6)
C
RV-GFP
RV-Ebf1
iLMP1
single cell outgrowth (%)
0/6
0/6
0/6
0/9
9/9
1/6
RV-GFP
RV-Ebf1
RV-Rel
αCD40/IL4
iLMP1
D
symptom-free survival (%)
days post transfer
αCD40/IL-4
RV-GFP 3*10^5(n=2)/10^3(n=2)
RV-Ebf1 3*10^5(n=2)/10^3(n=2)
RV-Rel 3*10^5 (n=2)/10^3(n=2)
iLMP1
RV-GFP 3*10^5(n=4)/10^3(n=2)
RV-Ebf1 3*10^5(n=5)/-10^3(n=9)
RV-Rel 3*10^5(n=5/-10^3(n=4)
E
liver
spleen
RV-GFP
RV-Ebf1
RV-Rel
1cm
iLMP1
F
spleen
iLMP1
RV-GFP
iLMP1
RV-Ebf1
iLMP1
RV-Rel
RV-GFP
LMP1 (huCD2) - PE-Cy7
G
spleen
liver
total reporter+ cells x 10^6
RV-GFP
RV-Ebf1
RV-Rel
αCD40/IL4
iLMP1
αCD40/IL-4
iLMP1
H
human tonsil
germinal center
B cells
CD40-L/IL-21
day 2 : RV-transduction
CD40-L/IL-21
day5:withdraw
CD40-L/IL-21
analysis
cell count (day12/day5)
p=0.0656
lg2(cell count over RV-LMP1)
RV-GFP
RV-Ebf1
RV-Rel
RV-LMP1
RV-LMP1/RV-Ebf1
RV-LMP1/RV-Rel

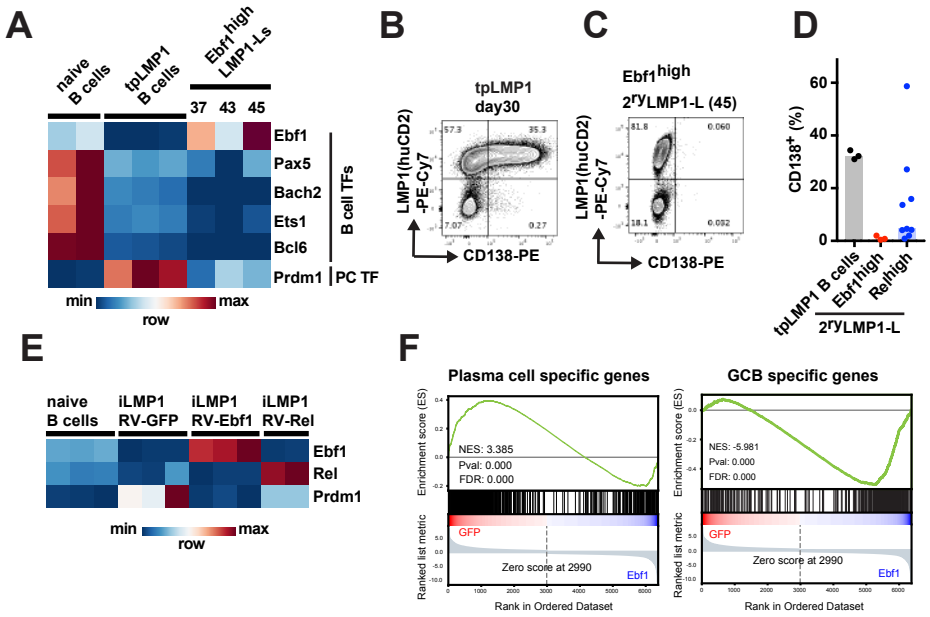
A
naive B cells
tpLMP1 B cells
Ebf1 high LMP1-Ls
37 43 45
Ebf1
Pax5
Bach2
Ets1
Bcl6
Prdm1
B cell TFs
PC TF
min
max
row
B
tpLMP1 day30
LMP1(huCD2) -PE-Cy7
CD138-PE
57.3
35.3
7.07
0.27
C
Ebf1high 2ryLMP1-L (45)
LMP1(huCD2) -PE-Cy7
CD138-PE
81.8
0.060
18.1
0.092
D
CD138+ (%)
60
40
20
0
tpLMP1 B cells
Ebf1high
Relhigh
2ryLMP1-L
E
naive B cells
iLMP1 RV-GFP
iLMP1 RV-Ebf1
iLMP1 RV-Rel
Ebf1
Rel
Prdm1
min
max
row
F
Plasma cell specific genes
GCB specific genes
Enrichment score (ES)
NES: 3.385
Pval: 0.000
FDR: 0.000
NES: -5.981
Pval: 0.000
FDR: 0.000
GFP
Zero score at 2990
Ebf1
Ranked list metric
Rank in Ordered Dataset

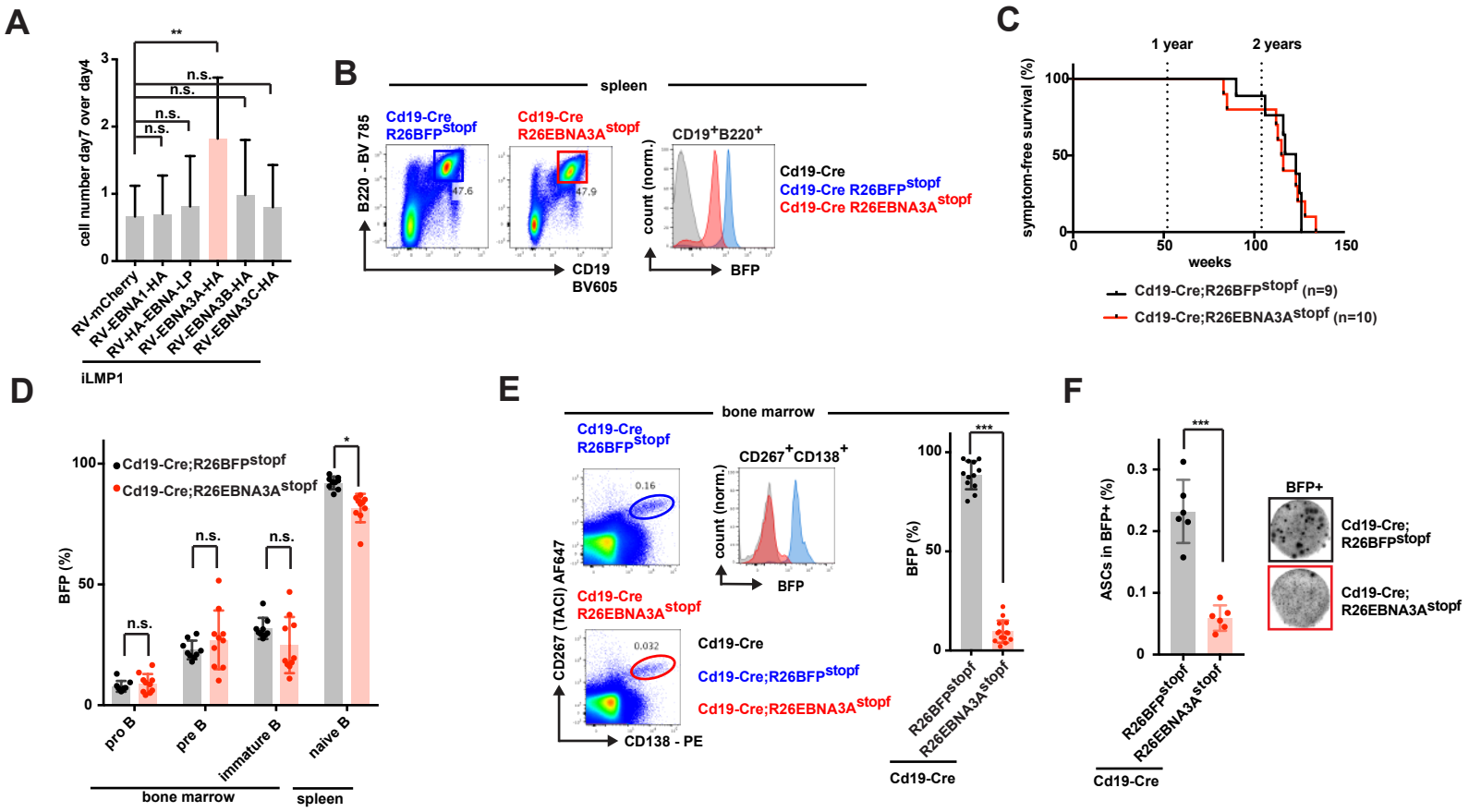
A
cell number day7 over day4
RV-mCherry
RV-EBNA1-HA
RV-HA-EBNA-LP
RV-EBNA3A-HA
RV-EBNA3B-HA
RV-EBNA3C-HA
iLMP1
B
spleen
Cd19-Cre R26BFPstopf
Cd19-Cre R26EBNA3Astopf
CD19+B220+
B220 - BV 785
CD19 BV605
count (norm.)
BFP
Cd19-Cre
Cd19-Cre R26BFPstopf
Cd19-Cre R26EBNA3Astopf
C
1 year
2 years
symptom-free survival (%)
weeks
Cd19-Cre;R26BFPstopf (n=9)
Cd19-Cre;R26EBNA3Astopf (n=10)
D
Cd19-Cre;R26BFPstopf
Cd19-Cre;R26EBNA3Astopf
BFP (%)
pro B
pre B
immature B
naive B
bone marrow
spleen
E
bone marrow
Cd19-Cre R26BFPstopf
Cd19-Cre R26EBNA3Astopf
CD267+CD138+
count (norm.)
BFP
CD267 (TACI) AF647
CD138 - PE
Cd19-Cre
Cd19-Cre;R26BFPstopf
Cd19-Cre;R26EBNA3Astopf
BFP (%)
R26BFPstopf
R26EBNA3Astopf
Cd19-Cre
F
ASCs in BFP+ (%)
BFP+
Cd19-Cre; R26BFPstopf
Cd19-Cre; R26EBNA3Astopf
R26BFPstopf
R26EBNA3Astopf
Cd19-Cre

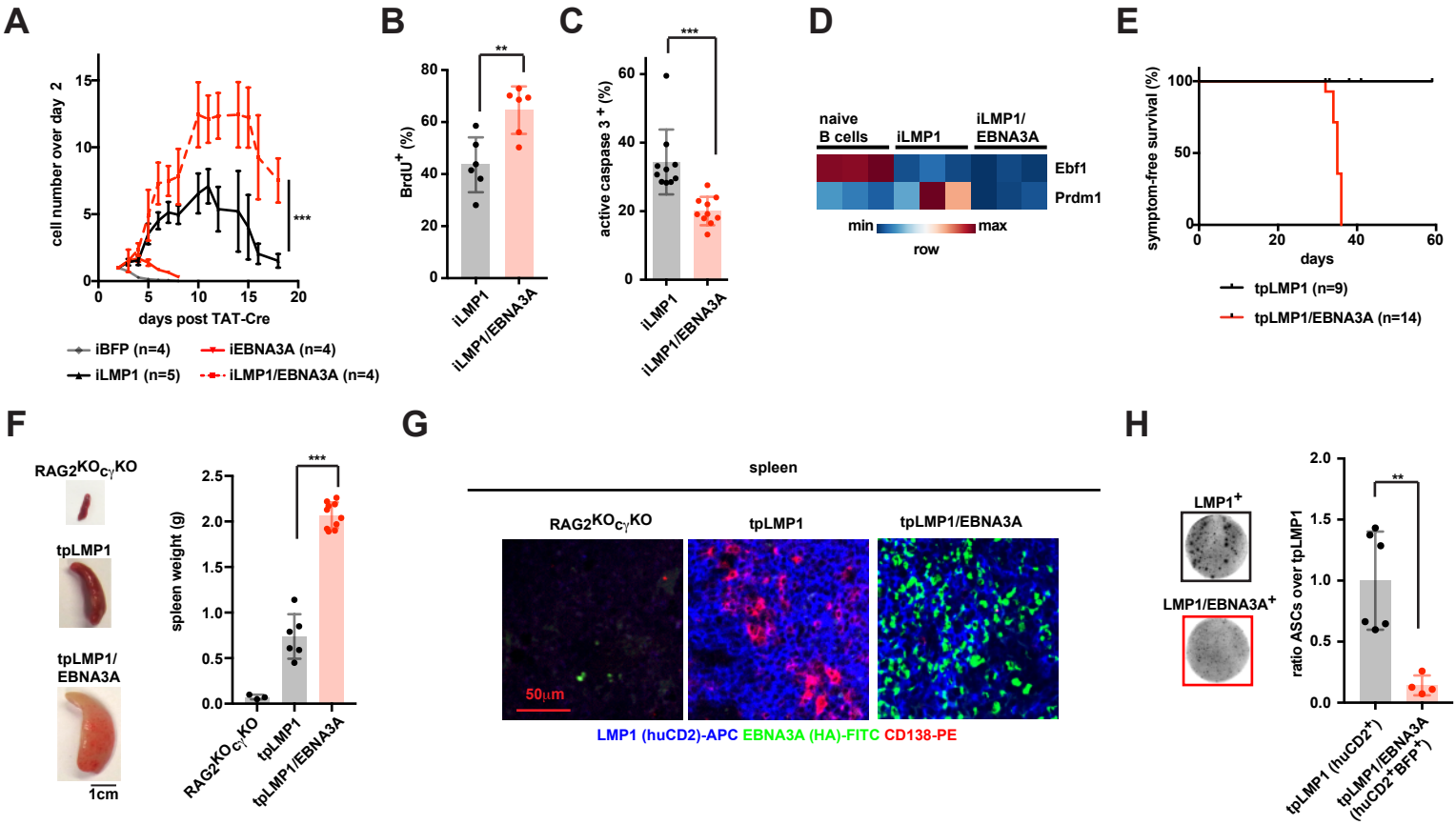
A
cell number over day 2
days post TAT-Cre
***
iBFP (n=4)
iEBNA3A (n=4)
iLMP1 (n=5)
iLMP1/EBNA3A (n=4)
B
BrdU+ (%)
**
iLMP1
iLMP1/EBNA3A
C
active caspase 3 + (%)
***
iLMP1
iLMP1/EBNA3A
D
naive B cells
iLMP1
iLMP1/ EBNA3A
Ebf1
Prdm1
min
max
row
E
symptom-free survival (%)
days
tpLMP1 (n=9)
tpLMP1/EBNA3A (n=14)

F
RAG2KOcγKO
tpLMP1
tpLMP1/ EBNA3A
1cm
spleen weight (g)
***
RAG2KOcγKO
tpLMP1
tpLMP1/EBNA3A
G
spleen
RAG2KOcγKO
tpLMP1
tpLMP1/EBNA3A
50μm
LMP1 (huCD2)-APC EBNA3A (HA)-FITC CD138-PE
H
LMP1+
LMP1/EBNA3A+
ratio ASCs over tpLMP1
**
tpLMP1 (huCD2+)
tpLMP1/EBNA3A (huCD2+BFP+)

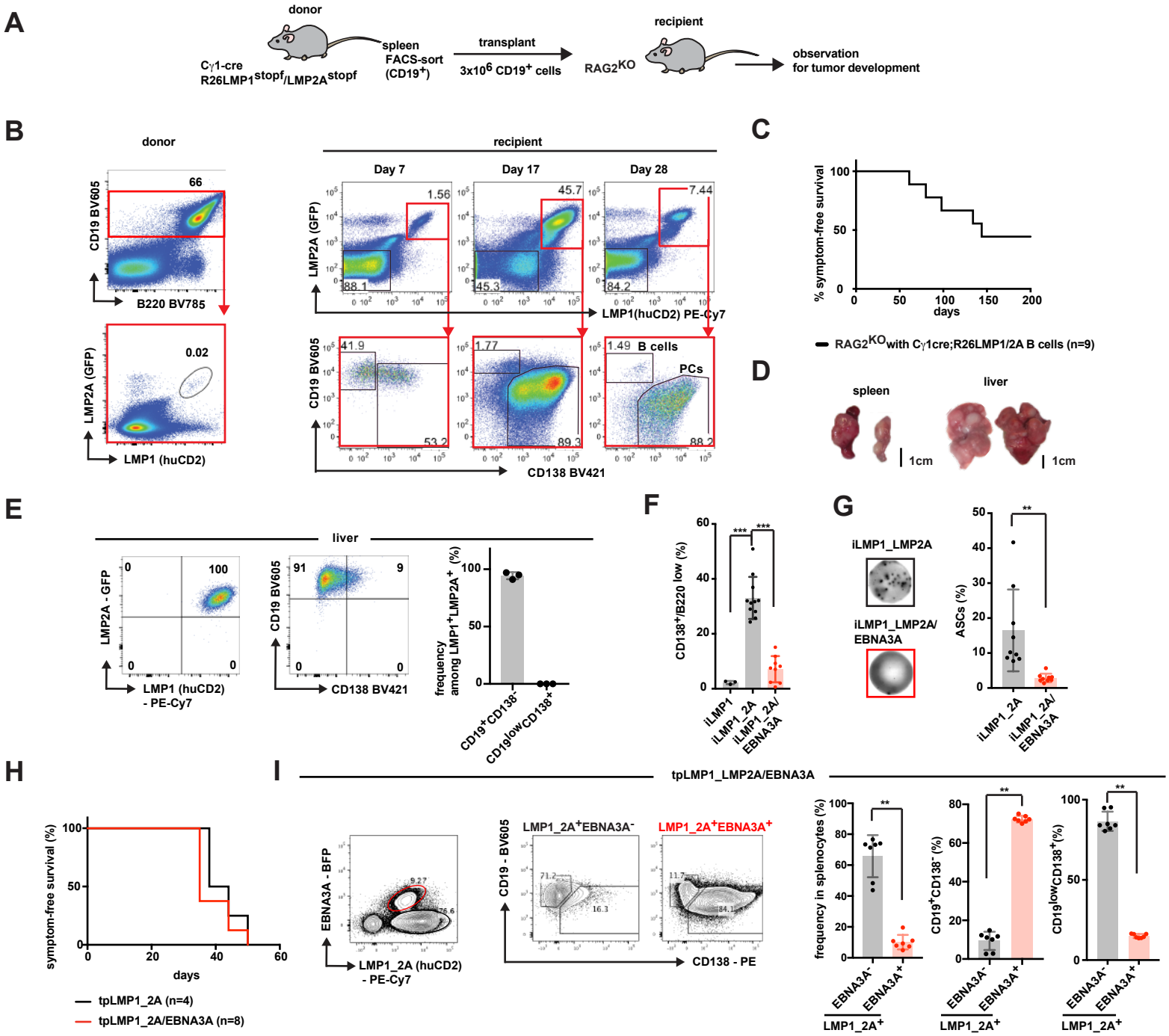
A
donor
Cγ1-cre
R26LMP1stopf/LMP2Astopf
spleen
FACS-sort
(CD19+)
transplant
3x10^6 CD19+ cells
RAG2KO
recipient
observation
for tumor development
B
donor
recipient
Day 7
Day 17
Day 28
CD19 BV605
B220 BV785
66
LMP2A (GFP)
0.02
LMP1 (huCD2)
1.56
45.7
7.44
88.1
45.3
84.2
LMP1(huCD2) PE-Cy7
41.9
1.77
1.49
B cells
PCs
53.2
89.3
88.2
CD138 BV421
C
% symptom-free survival
days
RAG2KOwith Cγ1cre;R26LMP1/2A B cells (n=9)
D
spleen
liver
1cm
1cm
E
liver
LMP2A - GFP
LMP1 (huCD2)
- PE-Cy7
CD19 BV605
CD138 BV421
frequency among LMP1+LMP2A+ (%)
CD19+CD138-
CD19lowCD138+
F
CD138+/B220 low (%)
iLMP1
iLMP1_2A
iLMP1_2A/
EBNA3A
G
iLMP1_LMP2A
iLMP1_LMP2A/
EBNA3A
ASCs (%)
iLMP1_2A
iLMP1_2A/
EBNA3A
H
symptom-free survival (%)
days
tpLMP1_2A (n=4)
tpLMP1_2A/EBNA3A (n=8)
I
tpLMP1_LMP2A/EBNA3A
EBNA3A - BFP
LMP1_2A (huCD2)
- PE-Cy7
LMP1_2A+EBNA3A-
LMP1_2A+EBNA3A+
CD19 - BV605
CD138 - PE
frequency in splenocytes (%)
CD19+CD138- (%)
CD19lowCD138+(%)
EBNA3A-
EBNA3A+
LMP1_2A+

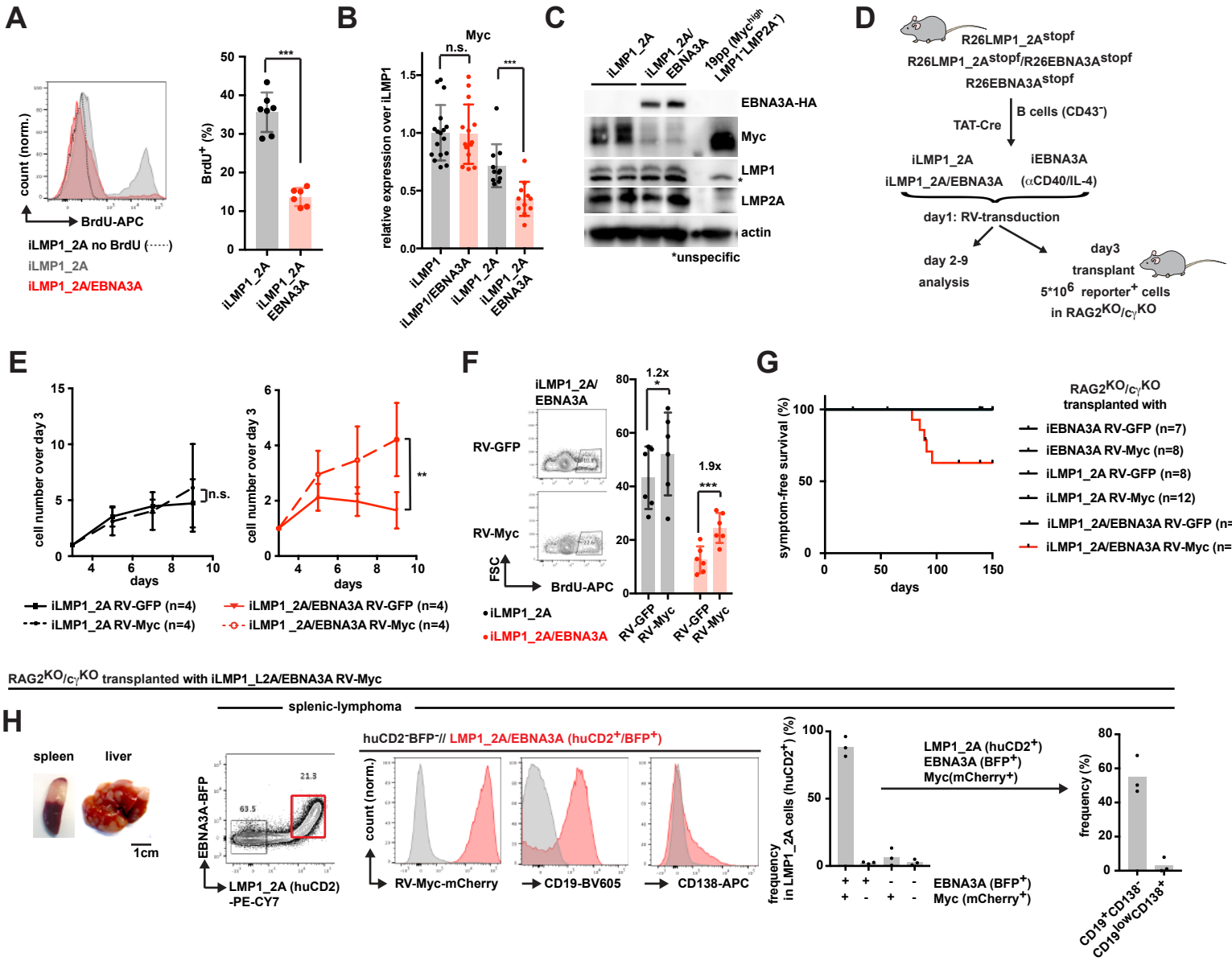
A
count (norm.)
BrdU-APC
iLMP1_2A no BrdU (·····)
iLMP1_2A
iLMP1_2A/EBNA3A
BrdU+ (%)
***
iLMP1_2A
iLMP1_2A EBNA3A
B
Myc
n.s.
***
relative expression over iLMP1
iLMP1
iLMP1/EBNA3A
iLMP1_2A
iLMP1_2A EBNA3A
C
iLMP1_2A
iLMP1_2A/ EBNA3A
19pp (Myc^high LMP1^-LMP2A^-)
EBNA3A-HA
Myc
LMP1
LMP2A
actin
*unspecific
D
R26LMP1_2A^stopf
R26LMP1_2A^stopf/R26EBNA3A^stopf
R26EBNA3A^stopf
TAT-Cre
B cells (CD43^-)
iLMP1_2A
iLMP1_2A/EBNA3A
iEBNA3A
(αCD40/IL-4)
day1: RV-transduction
day 2-9
analysis
day3
transplant
5*10^6 reporter^+ cells
in RAG2^KO/cγKO
E
cell number over day 3
days
n.s.
**
iLMP1_2A RV-GFP (n=4)
iLMP1_2A RV-Myc (n=4)
iLMP1_2A/EBNA3A RV-GFP (n=4)
iLMP1 _2A/EBNA3A RV-Myc (n=4)
F
iLMP1_2A/ EBNA3A
RV-GFP
RV-Myc
FSC
BrdU-APC
iLMP1_2A
iLMP1_2A/EBNA3A
1.2x
*
1.9x
***
RV-GFP
RV-Myc
G
symptom-free survival (%)
days
RAG2^KO/cγKO transplanted with
iEBNA3A RV-GFP (n=7)
iEBNA3A RV-Myc (n=8)
iLMP1_2A RV-GFP (n=8)
iLMP1_2A RV-Myc (n=12)
iLMP1_2A/EBNA3A RV-GFP (n=8)
iLMP1_2A/EBNA3A RV-Myc (n=14)
RAG2^KO/cγKO transplanted with iLMP1_L2A/EBNA3A RV-Myc
H
splenic-lymphoma
spleen
liver
1cm
EBNA3A-BFP
LMP1_2A (huCD2) -PE-CY7
huCD2^-BFP^-// LMP1_2A/EBNA3A (huCD2^+/BFP^+)
count (norm.)
RV-Myc-mCherry
CD19-BV605
CD138-APC
frequency in LMP1_2A cells (huCD2^+) (%)
LMP1_2A (huCD2^+)
EBNA3A (BFP^+)
Myc(mCherry^+)
EBNA3A (BFP^+)
Myc (mCherry^+)
frequency (%)
CD19^+CD138^-
CD19^lowCD138^+

Supplemental Appendix:

Supplemental Material and Methods

Mouse strains and handling

Rag2^{KO}cγ^{KO} mice used as recipients the initial LMP1-lymphoma cohort (Fig. 1A) had a C57BL/6J x C57BL/10SgSnAi genetic background (Taconic). All other mice were generated on or backcrossed for more than 10 generations to C57BL/6. Up to 6 mice per cage were housed under specific pathogen–free conditions (FELASA) in individually ventilated cages in a room illuminated in a 12h light-dark cycle, with access to water and autoclaved standard pellet chow ad libitum. All cages contained 5mm of aspen chip and tissue wiles for bedding and a mouse house. Experimental mice were fed with acidified water pH [2.5-3].

Cell culture

Cells were cultured at 37°C and 5% CO_2 in a humidified incubator. Unless noted otherwise, cell culture media and supplements were purchased from Thermo Fisher. PLAT-E (cell biolabs) and CD40-L/BAFF feeder cells (40LB) (1) were grown in standard culture medium (SCM - glutamine, pyruvate and glucose containing (full) DMEM supplemented with 10% FCS. Mouse embryonic fibroblasts (MEF) were grown in MEF-Medium (MEFM - full DMEM supplemented with 10% FCS, 1x non-essential amino acids (NEAA), 1x Penicillin/Streptomycin (Pen/Strep) and 1x GlutaMAX). LMP1-lymphoma cell lines were cultured in 15% B cell medium (BCM15 - full DMEM with 15% FCS, 1x GlutaMAX, 100mM HEPES , 1x NEAA, 1x Pen/Strep and 52µM β-mercaptoethanol (β-Me)). Primary mouse B cells and 19pp mouse Burkitt lymphoma cell line (2) were cultured in 10% B cell medium (BCM10 - full DMEM with 10% FCS, 100mM HEPES, 1x NEAA, 1x Pen/Strep and 52 µM β-Me). Mouse embryonic stem cells (ES-cells) were cultured in ES-cell medium (ESM - KnockOut™ DMEM - supplemented with 15% FCS, 1x NEAA, 2mM L-glutamine, 300U/mL ESGRO/LIF (Merck) and 100µM β-Me).

MEF isolation

MEFs were isolated according to standard procedures (3). MEFs in passage 3 were treated with 10µg/ml mitomycin (Sigma) for 2h at 37°C and subsequently washed 2x with PBS. In the manuscript MMC-treated passage 3 MEFs are referred to as MEFs.

Embryonic stem cell culture and targeting

R26-targeting vectors were digested with AsiSI (NEB) at 37°C overnight. Linearized-DNA was purified by 2x Phenol:Chlorophorm:Isoamylalcohol (25:24:1) and 1x Chloroform extraction. DNA was precipitated with 0.1vol 3M NaOAc and 2vol of Ethanol at -20°C over night. DNA was washed with 70% Ethanol and dissolved in H_2O to a concentration of 0.5µg/µl. ES-cells were cultured on MEFs in ESM on gelatin-coated tissue culture plates to maximum sub-confluency and medium was changed daily. For electroporation, ES-cells were washed 1x with PBS [pH 7.4] and trypsinized. Trypsinized cells were washed 1x with PBS [pH 7.4] and resuspended in RPMI 1640 without phenol red (Thermo Fisher) to a

density of 1.25 x 10^7 cells/ml. 1x10^7 cells were then electroporated with 25µg linearized targeting vector using a GenePulser (Biorad - 0.4cm cuvettes, 230V and 500µF). Electroporated cells were cultured on 2-3 MEF-coated 10cm-dishes. 24h post electroporation ESM was supplemented with 200µg/mL G418. After 7 days G418 (Sigma) resistant colonies were picked, dissociated with 1x Trypsin supplemented with 1% chicken serum and expanded on MEF-coated plates in G418-ES-medium. Expanded ES-cell clones were analyzed for correct integration by southern blot.

Blastocyst injection

On the day of blastocyst injection sub-confluent ES-cells were detached using ESGRO accutase (Merck) for 5min at 37°C. Detached cells from one 10cm dish were transferred in 5ml G418-free ESM to gelatin-coated 6cm-dish for 15min at 37°C to allow attachment of MEFs. ES-cells in the supernatant were collected, pelleted and resuspended in 1ml injection buffer (full DMEM with 10% FCS, 100mM HEPES, 1x Pen/Strep and 300U/ml DNAse (Sigma)). Blastocyst injection of ES-cells was performed in the transgenic core facility of the MDC according to standard protocol.

Cell preparation from mouse organs

Cells from spleen, liver and tumors were prepared by grinding the organ/tumor between two frosted object slides in B cell prep medium (BPM - full DMEM supplemented with 1% FCS and 1mM EDTA). Bone marrow was prepared by flushing femur and tibia with BPM using a syringe. Single cell suspensions were depleted for red blood cells by resuspending cells 500µl BPM and mixing them with 5ml Gey solution [3.5mL H2O, 1mL Gey A (35g/L NH_4Cl, 1.85 g/L KCl, 1.5g/L Na_2HPO_4 x 12 H2O, 0.12g/L KH_2PO_4, 5g/L glucose, 50 mg/L phenol red), 0.25mL Gey B (4.2g/L $MgCl_2$ x 6 H_2O, 1.4g/L $MgSO_4$ x 7 H_2O, 3.4g/L $CaCl_2$), 0.25mL Gey C (22.5g/L $NaHCO_3$)]. After 3min lysis was stopped with 5ml BPM. Cells passed through a 70µm filter, pelleted (8min; 1200rpm), resuspended in BPM and counted with a casy-cell counter (OLS). To deplete non-B cells, splenic cells were incubated with anti-CD43 MACS-beads (Miltenyi- 40µl beads in 600µl BPM) for 25min on ice. Labeled cells were washed with 10ml BPM and pelleted. Cells were resuspended in BPM and passed through magnetic LR-columns (Miltenyi). $CD43^-$ B cells in the flow through were pelleted and resuspended in BCM10.

HSPC transplant

$Rag2^{KO}c\gamma^{KO}$ mice were xray-irradiated (3gy) using a RS-2000 (Radsource). 3 days before up until 14 days post irradiation, mice were fed 0.2% Neomycin-sulfat (bela-pharm) in the drinking water. 24h post irradiation mice were iv-injected with 1000 FACS-sorted fetal liver (E16.5) $Lineage^-Sca^+c\text{-}Kit^+$ LSK cells (referred to as HSPCs) and 1*10^6 *$Rag2^{KO}c\gamma^{KO}$* bone marrow carrier cells in PBS supplemented with 2% FCS (lineage markers: B220, CD19, Ter119, CD11b, CD11c, Gr1.1. and CD3ε). HSPCs for reconstitution were derived from at least 2 independent fetal donors.

Cell and tumor transfer

Single cell suspensions in 2% FCS (Thermo Fisher) in PBS were injected into the tail vein of recipient mice. Cγ1-Cre;LMP1/2A B cells were FACS-sorted ($CD19^+$) before transfer. RV-transduced B cells were transplanted as bulk (i.e. mix of transduced and non-transduced cells). Indicated numbers of transplanted cells in the figures represent total transduced $reporter^+$ cells that were transferred. Cells from at least 2 independent donors were used.

TAT-Cre treatment

B cells were washed 3x with PBS at 4°C and incubated with 60μg TAT-Cre (4) in Hyclone media (Thermo Fisher) at 37°C for 40min. When indicated, cells were retrovirally transduced 24h after TAT-Cre treatment. B cells expressing TAT-Cre induced transgenes are referred to as i("*transgene"*) B cells.

B cell stimulation and plasma blast-differentiation in vitro

B cells were stimulated with 2μg/ml LEAF-purified αCD40-antibody (Biolegend) and 20ng/ml IL-4 (R&D systems). To differentiate B cells in plasma blasts, αCD40/IL-4 stimulated cells were washed on day 2 with PBS and cultured on irradiated (12 gray) 40LB feeder cells in the presence of 20ng/ml IL-21 (R&D systems). When indicated, cells were retrovirally transduced 24h after stimulation.

Retroviral transduction

PLAT-E MSCV-packaging cells were transfected with MSCV-vectors using Fugene (Promega) according to the manufacturer's instructions. 24h post transfection medium was exchanged. 48h post transfection virus containing PLAT-E supernatant was collected and sterile filtered (0.45μm). For viral transduction, tissue culture dishes were coated with 50 μg/ml retronectin (Takara) at 4°C over-night. Coated dishes were washed with PBS and blocked with 2% BSA in PBS for 30min at RT. Blocked plates were incubated with PLAT-E-supernatant at RT for 30min. Cells were mixed 1:1 with PLAT-E-supernatant, transferred to virus-coated plates and spin-transduced at 2000 rpm/27°C for 90min in the presence of 4μg/ml polybrene (Sigma). 24h post transduction the medium was exchanged.

Single cell transformation

iLMP1 B cells or αCD40/IL-4-stimulated $CD43^-$ B cells from $R26LMP1^{stopf}$ mice were transduced with empty MSCV-ires-GFP or MSCV-ires-GFP encoding *Ebf1*-ires-GFP or *Rel*-ires-GFP 24h post TAT-Cre or stimulation. On day 3 single GFP^+ cells were FACS-sorted into MEF-coated 96-wells containing 100μl BCM15. After 2 weeks wells with outgrowing GFP^+ colonies were counted using a BZ 9000 fluorescence microscope (Keyence).

BrdU incorporation

In vitro cultured cells were incubated with 10μM BrdU (BD). After 16h life cells were labeled for 15min at RT by zombie aqua exclusion (Biolegend). Cells were fixed and BrdU was detected with a APC-BrdU FACS-labeling kit (BD) according to the manufacturer's instructions. BFP was detected by simultaneous staining with an Alexa 488-conjugated αGFP antibody (Thermo fisher). In experiments including BFP^+/GFP^+ double positive cells, all cells were FACS-sorted for reporter expression prior to the staining. Reporter staining was then excluded from the final analysis.

Active Caspase 3 staining

FACS-sorted $reporter^+$ cells were fixed and stained for active caspase 3 using a PE-Active caspase-3 apoptosis kit (BD) according to manufacturer's instructions.

Cell cycle analysis

FACS-sorted $reporter^+$ cells were washed with cold PBS and fixed with ice cold methanol (66% in PBS) for 2h. Fixed cells were pelleted and rehydrated with PBS for 15min. Rehydrated cells stained with 30μg/ml PI and 100μg/ml RNAse for 30min in PBS.

FACS staining, analysis and sorting

Cells were incubated with 10μg/ml TruStain fc-block (Biolegend) in FACS-buffer (PBS supplemented with 1% FCS, 1mM EDTA and 0.05% Sodium Azide) for 20min. Fc-blocked cells were stained with fluorophore- and/or biotin-labelled antibodies (1:200) in FACS-buffer for 30 min. Antibodies are listed in SI-Appendix Table A. Samples with biotin-labeled antibodies were washed 2x in FACS-buffer and stained with Streptavidin-conjugated fluorophores in FACS-buffer for 30 min. Stained cells were washed 1x with FACS-buffer and acquired with a FACS-Fortessa (BD). Human GCB cells were acquired on an LSRII (BD). Cell sorting was performed on an FACSAria (BD). FACS-files were analyzed using the FlowJo software (flow-jo). In all analysis dead cells were excluded by FSC/SSC (in vitro) or FSC/SSC and zombie aqua or PI exclusion (ex vivo). Cells analyzed were pre-gated for every indicated transgene. In iLMP1, iLMP1_2A, iLMP1/EBN3A and iLMP1_2A/EBNA3A cultures all blasting cells are $huCD2^+$, we therefore used, unless noted otherwise, blasting as a surrogate reporter for LMP1 or LMP1_2A expression. Cell counting of in vitro cultured cells was performed in FACS-analysis using counting beads.

Elispot

Multiscreen protein binding plates (Merck) were activated with 35% ethanol in PBS, washed with PBS and incubated with anti λ- and κ-light chain antibodies 1:1000 in PBS for 16h at 4°C. Plates were blocked with BCM10 for 30min at 37°C. $Reporter^+$ FACS-sorted cells were seeded on coated plates in BCM10 and incubated for 16h. Plates were washed 6x with PBS/0.1% Tween and incubated with biotin coupled anti λ- and anti κ-light chain antibodies in 1:500 PBS/0.1% Tween for 2h at 37°C. Plates were washed with deionized water and incubated with 1:3000 streptavidin-AP in PBS at RT of 30min. Plates were washed with deionized water and stained with BCIP/NBT color development substrate (Promega). Plates were imaged using immune-spot-imager (CTL) and large spots were counted by immune-spot-imager software (CTL). When freeze/thawed cells were used, the frequency of antibody

secreting cells (ASC) was presented as relative frequency over control cells. Elispot-antibodies can be found in SI-Appendix table A.

Western blot

Cell were lysed in RIPA buffer (20mM Tris-HCl [pH 7.5] ,150mM NaCl, 1mM EDTA, 1% NP-40, 0.1% SDS, 0.1% sodium Deoxycholate) supplemented with 1x c0mplete protease inhibitors (Sigma) for 20 min on ice. Nuclei were pelleted. Lysate was heated in 1x SDS-sample buffer for 3min at 96°C (6 x SDS-sample buffer; 250mM TRIS [pH 6.8], 38% glycerol, 10% SDS, 5% β-Me, 0.01% bromphenol blue). Proteins were separated by SDS-gel-electrophoresis and transferred to PVDF membranes. Membranes were blocked with 5% skim milk power in 1xTBST (50mM Tris [pH 7.6]; 150mM NaCl; 0.05% Tween 20). Primary antibodies were incubated 1:1000 in 1xTBST. Filtered supernatant from LMP1-antibody secreting hybridoma (S12) was incubated as is. Membranes were washed 5x with TBST and incubated with HRP-coupled secondary antibodies were at 1:10000 in 1x TBST. Membranes were imaged using ECL-solution (VWR) and a fusion SL–imager (Vilber). Images were trimmed and level corrected (without gamma correction) by Photoshop (Adobe). Antibodies are listed in SI-Appendix Table A.

HA-Co-immunoprecipitation

$10*10^6$ stimulated B cells were washed 2x with cold PBS and lysed in 500µl IP lysis buffer (0.5% Tween20, 25mM Tris [pH 8.0], 200mM NaCl, 2mM EDTA, 5mM NaF, 1mM sodium orthovanadate, 2mM Sodium Pyrophosphate, 1x c0mplete protease inhibitor) for 25min on ice. Nuclei were pelleted and supernatant was incubated with 10µl of Sepharose-A Dynabeads (Thermo Fisher) coupled to 5µl of anti-HA antibody (cell signaling) for 4h rotating at 4°C. Beads were washed 3x with IP lysis buffer at 4°C. Washed beads were boiled in SDS-sample buffer at 96°C for 5min.

Isolation of genomic DNA

gDNA was extracted using the DNeasy blood and tissue-kit (Quiagen) or Nucleo-spin tissue kit (Machery Nagel) according to the manufacturer's instructions.

PCR and Agarose gel extraction

PCR was performed on 100ng DNA using Herkulase (Agilent) or KOD-Polymerase (Merck) (for VDJ-PCR) and a according to the manufacturer's instructions. PCR fragments were isolated from agarose gels using a PCR-cleanup gel-extraction kit (Machery-Nagel). Primers are listed in SI-Appendix Table B.

CAS9 knockout efficiency estimation with the Inference of CRISPR Edits (ICE) tool

Sanger-sequencing files of PCR products spanning the sgRNA targeting-site in targeted and non-targeted controls were compared by Synthego-ICE-software to estimate KO-efficiency (https://ice.synthego.com) (5).

Southern blot

5µg of gDNA was fully digested with EcoRI, or PacI (both Promega) and separated by electrophoresis on a ethidium bromide containing 0.7% agarose gel in 1x TAE buffer (0.04M Tris, 0.02M acetic acid, 1mM EDTA). The DNA-gel was 2x washed in deionized water and incubated for 2x 15min in 0.125M HCl. Next, gel was washed 2x in deionized water and incubated in transfer buffer (1.5M NaCl /0.5M NaOH) for 2x 15min. DNA was transferred over night at RT with transfer buffer by southern blotting to a pre-activated (5min H_2O, 15min transfer buffer) Hybond-XL nylon-membrane (Amersham). After transfer, the membrane was neutralized for 10min in neutralization buffer (0.5M Tris [pH7.2], 1M NaCl). Membrane was dried, crosslinked to DNA with a UV-Crosslinker (Stratalinker) and incubated in Express-HYB (Takara) at 65°C for 30min. Radioactive probes were generated using ^{32}P-CTP and the Ladderman labelling kit (Takara) according to the manufacturer's instructions. Labeled probes were purified using ProbeQuant™ G-50 Micro Columns (GE) and denatured at 96°C for 5min followed by 5 min on ice. The membrane was incubated with the probe in ExpressHYB at 65°C for 18-24h. The excess probe and unspecific labelling was removed by washing the membranes 3 times with SSC buffers for 30 min at 65°C. 1st wash 2 x SSC (0.3M NaCl, 0.03M sodium citrate/0.1% SDS). 2nd wash 1 x SSC/0.1% SDS. 3rd wash 0.5 x SSC/0.1% SDS, respectively. Finally, the membrane was enclosed in a plastic foil and exposed to a CL-Xposure film (Thermo Fisher) at -80°C.

Probe sequences

R26/R4A	GAATTCATGTCACTTGCACTGGGAAAACAAAACAAAGATCCTCCT
	CACCCTATTACCCACATTACTATTTTTAGGTTTTTTAGGGGTTAAA
	AAAGATCAAAACACTAATGAACTTTAAGTCCTGTGAAGGGTAAAA
	CCTCAGATAGTAACAAAAAGCTTCCAACCCCTCCTCAAACAAAAA
	ACCCCAAGTCTTTAACTTTGATCCAGTTTTCAGATGCTGATATCC
	ATAAATGGATACAGTTATGAATTGCTAATTCTGGTCTCTTCACTA
	GCAAAAAGCAAAGCAGCTCAGCAGTACAATTTCCCAGGAAAGCA
	AGCAAGGTTTCTTTCCAGCCTGAGCAGCCATCACTAAGTGCAGT
	TCCCTGCAGCCAACAGCATTAATGGACGCTGCACTGCTGTCCTT
	CCCTGGAGACAGCAGCCAGCACTACTCAAGCTTCTCACGTAGCA
	ACCAGAGCTCCAGAGCCAGCAGCTGCTGCCGCCTTGTATACTCA
	CTCCTGTGATCCAACACAGGAGCAACCTTTTCTTTACCCCACCC
	CCACTTCTTAACACACTTTTTTTTGGGGGGGGGGGGGGAACAAGT
	GCTCCATGCTGGAAGGATTGGAACTATGCTTTTAGAAAGGAACA
	ATCCTAAGGTCACTTTTAAATTGAGGTCTTTGATTTGAAAATCAAC
	AAATACCAAATTCCAAATATTCGTTTTAATTAA
Neo	GGATCCGAACAAACGACCCAACACCCGTGCGTTTTATTCTGTCT
	TTTTATTGCCGATCCCCTCAGAAGAACTCGTCAAGAAGGCGATA
	GAAGGCGATGCGCTGCGAATCGGGAGCGGCGATACCGTAAAGC
	ACGAGGAAGCGGTCAGCCCATTCGCCGCCAAGCTCTTCAGCAA
	TATCACGGGTAGCCAACGCTATGTCCTGATAGCGGTCCGCCACA
	CCCAGCCGGCCACAGTCGATGAATCCAGAAAAGCGGCCATTTTC
	CACCATGATATTCGGCAAGCAGGCATCGCCATGGGTCACGACG
	AGATCCTCGCCGTCGGGCATGCGCGCCTTGAGCCTGGCGAACA
	GTTCGGCTGGCGCGAGCCCCTGATGCTCTTCGTCCAGATCATCC
	TGATCGACAAGACCGGCTTCCATCCGAGTACGTGCTCGCTCGAT
	GCGATGTTTCGCTTGGTGGTCGAATGGGCAGGTAGCCGGATCA
	AGCGTATGCAGCCGCCGCATTGCATCAGCCATGATGGATACTTT
	CTCGGCAGGAGCAAGGTGAGATGACAGGAGATCCTGCCCCGGC
	ACTTCGCCCAATAGCAGCCAGTCCCTTCCCGCTTCAGTGACAAC

GTCGAGCACAGCTGCGCAAGGAACGCCCGTCGTGGCCAGCCAC
GATAGCCGCGCTGCCTCGTCCTGCAG

JH GGCTCCCTCAGGGACAAATATCCAAGATTAGTCTGCAATGCTCA
GAAAACTCCATAACAAAGGTTAAAAATAAAGACCTGGAGAGGCC
ATTCTTACCTGAGGAGACGGTGACTGAGGTTCCTTGACCCCAGT
AGTCCATAGCATAGTAATCACAATAGTGGATTTTTCCTCTATACC
CGACAAAAACCCCAGAGTCTGACTAGAATCACCCCTGGGCAACT
CAGACATTATGCCAATTCCTGGTGTCACACAAGAATCAACCATTC
AAGTCATTGTTCCACATTCTGTTCCCTGCCTGTGCAGAAGCCCC
CTGGACCCCTCTTAAGTCTTCAAGGTGACCTATATTCCAGCCTCA
CCTCAGAGAAACCAGACAGTCACTGACCCTGAAATTGTCACCAT
CAACTGTCAGCCCCTAATTCTCACAAGAGTCCGATAGACCCTGG
ACAAGATTCTGCCTCAGACTTCAAGCT

Array CGH

Sample gDNA was derived from 2^{ry}LMP1 lymphomas FACS-sorted for huCD2 expression. Tail-DNA was derived from flHSPC-donor fetuses. Array CGH was performed and analyzed as described before (6). In brief 250ng of genomic DNA of tumor and tail-DNA of donor animal were labelled with Cy3-dCTP and Cy5-dCTP, respectively using the Cytag kit (Enzo). The labelled nucleotides were purified using Microcon xym-30 columns (Merck) prior hybridization onto mouse 8 x 60k array CGH arrays (Agilent) with the design ID 82410 followed by washing and scanning according to the manufacturer's protocol.

Library preparation for exome sequencing

Exome-libraries of gDNA were created with the SureSelect (XT) Mouse All Exon Kit, according to the manufacturer's instructions and sequenced on an Illumina NextSeq 500.

SNP calling from exome sequencing

Paired-end reads were mapped to the mm10 reference genome (ftp-mouse.sanger.ac.uk/ref/GRCm38_68.fa) using bwa-mem(7). In BAM files PCR duplicates were marked, read groups were added, and reads were realigned locally around indels. After local re-alignments, pair mate information was fixed and read scores calibrated using Picard tools version 1.141 (Broad Institute). Reads from different lanes were merged to a single BAM file per sample, and PCR duplicates were removed again. Mutations were called using MuTect version 1.1.7 (8) by comparing tumor samples to tail-samples of the fHSC-donor fetus. Most deleterious mutation effects were predicted using the Ensembl Variant Effect Predictor (VEP) (9). Variants with an allele frequency above 0.35 were considered as clonal.

Translocation mapping from exome sequencing

Genomic fusions were identified in exome sequencing reads using FACTERA version 1.4.4 (10), using the mm10 reference genome from Sanger and the following parameters:

Minimum breakpoint-spanning reads for each fusion (r): 5
Minimum discordant reads for each candidate fusion (m): 2
Maximum breakpoints to examine for each read pair (x): 5

Minimum reads with same breakpoint required (s): 1
Minimum fraction of read bases for fusion template alignment (f): 0.9
Minimum % similarity for read to match fusion template (S): 0.95
K-mer size for fragment comparison (k): 12
Minimum size of soft-clipped read region (c): 16
Number of bases flanking breakpoint for fusion template (b): 500
Number of threads for blastn search (p): 4
Number of bases flanking breakpoint to provide in output (a): 50

The results were filtered for translocations with one end within chr12: 113,153,879 - 116,047,724 (Igh-locus) or chr6: 67,491,855 - 70,765,720 (Igk-locus) or chr16: 18,970,309-19,284,104 (Igl-locus).

RNA-extraction

RNA was isolated by RNeasy kit (Quiagen) including a DNAse digestion step according to the manufacturer's instruction.

RT-qPCR

RNA was transcribed into cDNA by superscript III (Thermo Fisher) using random hexamer primers according to the manufacturer's instructions. 5-8ng of cDNA of FACS-sorted cells was amplified using a Power-SYBR-Green RT-PCR-kit (Thermo Fisher) and a STEP-ONE-PLUS RT-qPCR-cycler (Applied Biosystems). Analysis was done by ΔΔCT-method, using HPRT as a housekeeping control gene. Every data point represents the mean of 2-3 technical replicates in one biological replicate. Primers are listed in SI-Appendix Table B.

Library preparation for RNA-sequencing

For RNA-sequencing of tumor samples, RNA was isolated from FACS-sorted (huCD2$^+$) non-transformed tpLMP1 B cells (day 18-20 post transplantation), FACS-sorted (huCD2$^+$) 2^{ry}LMP1 lymphomas, or FACS-sorted (CD19$^+$/CD38$^+$/FAS$^-$) naïve splenic B cells from C57BL/6. RNAseq libraries were prepared with the TruSeq Stranded mRNA kit (Illumina), and 50bp single end sequencing was performed on a HiSeq™ 2000 Sequencing System (Illumina). For RNA-sequencing of in vitro cultured cells, RNA was isolated from FACS-sorted (reporter$^+$) B cells at day 6 post tat-cre, or FACS-sorted (CD19$^+$/CD38$^+$) naïve splenic B cells from C57BL/6 mice. RNAseq libraries were prepared using the NEBNext® Ultra™ II Directional RNA Library Prep Kit for Illumina (NEB) and was sequenced in a 2x76 cycle run on a HiSeq 4000 (Illumina).

RNA-sequencing analysis

Reads were mapped and gene expression quantified using PiGX (11), an integrated pipeline for read trimming, mapping, quality control, and gene expression quantification. Reads counts assigned to genes were transformed using a variance stabilizing transform (VST) (12) with the DESeq2 R package (version 1.22.2) (13) using R version 3.5.1. The gene expression matrix was filtered to only include genes with at least one read in one of the samples. Principal component analysis was performed using the 500 genes with the highest variance (in VST). Xist and immunoglobulin heavy and light chain genes were excluded from the principal component analysis to avoid biasing the results by gender or Ig-usage.

Gene set enrichment analysis

Gene expression data for mouse splenic plasma cells (SplPC) and germinal center B cells (GCBC) from Shi et al. (14) were downloaded from the gene expression omnibus (GSE60927). Differential expression analysis was run using DESeq2, contrasting SplPC with GCBC. SplPC-induced genes were identified as genes with log2 fold change above 2, and SplPC-repressed genes (GCBC-specific genes) were identified as genes with log2 fold change below 0.5. Immunoglobulins variable genes and Xist were excluded. DESeq2 was also done contrasting *Ebf1*- and GFP-expressing iLMP1 B cells on day 6 post TAT-Cre. Genes with an adjusted P value below 0.005 were kept. Selected genes were then ordered by their log2 fold change to generate the ranked gene list for GSEA. Immunoglobulin variable genes and Xist were excluded.

The ranked gene lists and induced/repressed gene sets were then input to the GSEApy package (version 0.9.13,https://github.com/zqfang/GSEApy) and analyzed using the GSEAPreranked module.

Analysis of NF-κB target genes

LMP1/NF-κB targets-genes previously defined by Cahir-McFarland et al (15) were used to cluster samples using VST counts (DESeq2), using euclidean distances and average linkage. Z scores were computed by subtracting from each sample the population mean and dividing by the gene's standard deviation.

Cloning of MSCV-expression vectors

pMIGR1 (MSCV-ires-GFP) (16) and pMIB (MSCV-ires-BFP) were a kind gift from Martin Janz (Charite Berlin). MSCV-ires-mCherry was derived from MSCV-ires-GFP by substituting the eGFP-ORF (NcoI/SalI-fragment) with mCherry-ORF. MSCV destination vectors were created by inserting a gateway destination cassette into the XhoI-site upstream of the ires. ORFs of EBV/B95-8 EBNA1, EBNA-LP, EBNA3A, 3B and 3C were a kind gift of Elliott Kieff and Benjamin Gewurz an Bo Zhao (Harvard Medical School, Boston). EBV/B95-8 EBNA2 ORF was a kind gift of Wolfgang Hammerschmidt (Helmholtz Zentrum, München). Mouse *Myc*-, *Rel*- and *Ebf1*-ORFs were cloned from splenic cDNA from C57BL/6 mice. A HA-tag (TAC CCA TAC GAT GTT CCA GAT TAC GCT) was inserted via PCR with overhanging primers 5' of the EBNA1-, EBNA2-, EBNA3A-, 3B- and 3C-ORFs and 3' of the EBNALP-ORF. PCR-amplicons of all ORFs were cloned into pENTR entry vectors by pENTR/D-TOPO cloning kit (Thermo Fisher) and shuttled into MSCV destination vectors by LR-recombination with Gateway LR Clonase II (Thermo Fisher). Guide RNAs were expressed from MSCV-pU6-(BbsI)-CcdB-(BbsI)-Pgk-Puro-T2A-BFP (MSCV-sg-BFP) (17) and MSCV-pU6- (BbsI)-CcdB-(BbsI)-Pgk-Puro-T2A-mCherry (MSCV-sg-mCherry). MSCV-sg-mCherry was derived from MSCV-sg-BFP by substituting the BFP-ORF with an mCherry-ORF. sgRNAs were designed by CrispRGold (17) and inserted into the BbsI-site of MSCV-vectors. sgRNA sequences are indicated in supplemental information appendix table S2.

Cloning of Rosa26 targeting vectors

EBV/B95-8 ORFs of LMP1 and LMP2A were derived from gDNA of R26LMP1^{stopf} and R26LMP2A^{stopf} transgenic mice (18). The LMP1t2aLMP2A ORF was created by overlap-extension PCR, inserting a sequence encoding t2a self-cleavage peptide (gagggcagaggaagtctgctaacatgcggtgacgtcgaggagaatcctggacct) between LMP1 and LMP2A

ORFs. The STOP codon of LMP1 was eliminated in the 2A-construct. The LMP1t2aLMP2A-ORF was inserted into a pENTR vector by pENTR/D-TOPO cloning kit (Thermo Fisher). pR26-huCD2-Dest was created by inserting a gateway destination cassette into the PacI-site of pR26-huCD2 (2). Targeting vectors pR26-LMP1t2ALMP2A-ires-huCD2^{stopf} and pR26CAG-EBNA3A-HA-ires-BFP^{stopf} were created using LR Clonase II (Thermo Fisher) to shuttle ORFs from pENTR-LMP1t2aLMP2A and pENTR-EBNA3AHA into pR26-huCD2-Dest and pR26-CAG/BFP-Dest (19), respectively. To generate pR26-BFP-ires-huCD2^{stopf}, the ORF of eBFP2 was cloned into the AscI-site of pR26-huCD2. The eBFP2 template was derived from MSCV-ires-BFP.

Histology

Histology staining was performed and graded by the pathology core facility of the Universitätsklinikum Heidelberg. Organs were fixed with formalin (Sigma) for at least 48h. After fixation, representative specimens of spleen, liver and lung were routinely dehydrated, embedded in paraffin, and cut into 4-mm-thick sections. Sections were stained with an Autostainer (Dako) using standard conditions. In brief, sections were deparaffinated by sequential incubation in Xylol (2x10min), 100% Ethanol (2x5min), 96% Ethanol (2x5min), 70% Ethanol (2x5min) and then transferred to H_20. Sections were boiled in a pressure cooker in pH 6-Buffer (Dako) for 10min. After sections were chilled for 30min in in pH 6-Buffer. Sections were than boiled for 10min in in pH 9-buffer (Dako) at normal pressure and subsequently chilled for 30min. Sections were stained with primary antibodies BCL6 (ProteinTech Europe), IRF4/Mum1 (ProteinTech Europe) and CD10 (St. John's Laboratory) diluted in antibody diluent (Dako) for 30min. Sections were washed with TBS/Tween and incubated with secondary antibody (1:200 in antibody diluent) for 20min. Sections were washed with TBS/Tween and stained with "REAL Detection System" (DAKO) according to the manufacturer's instructions. For counterstain sections were incubated with 5min Hämalaun nach Mayer, followed by 5 min of H_2O. samples were than mounted in Auatex (Merck) and imaged with a NanoZoomer whole slide imager (Hamamatsu). Used antibodies are listed in SI-Appendix Table A.

Immunofluorescence and immunohistology

Cryostat-sections of OCT (Tissue-Tek) embedded organs were fixed with 100% acetone for 20min at RT. Sections stained for c-Rel were fixed 2h in 4% Paraformaldehyde in PBS, washed with PBS and fixed again with 100% Acetone for 20 min. Cultured cells were settled in PBS on Poly-D-lysine coated object slides and fixed with ice-cold methanol/acetone (1:1 vol/vol) for 2min. Fixed sections or cells were rehydrated in PBS for 15min and blocked with 2% BSA in PBS for 30min. Sections for c-Rel detection were blocked and permeabilized for 2h with 1% Triton-X100 in 3% BSA/PBS. Primary antibodies were incubated in PBS 0.2% BSA for 16h at 4°C. Sections were washed with PBS and incubated with secondary or fluorophore conjugated antibodies in PBS 0.2% BSA for 2-16h at RT. Slides were washed and incubated with 1µg/ml DAPI in PBS. Stained sections were mounted with Flouromount (Sigma) and imaged with a BZ-9000 microscope (Keyence). Images were trimmed and level corrected (no gamma correction) by Photoshop (Adobe). Images shown in the same panel were identically acquired and processed. Used antibodies are listed in SI-Appendix table A.

Multiplex-FISH (M-FISH)

To create metaphase spreads LMP1-lymphoma cell lines were cultured in 135ng/ml colcemid (Thermo Fisher) for 4h at 37C°. Cells were resuspended in 200µl PBS. 10ml hypertonic buffer (37.5mM KCl, 0.5% Sodium Citrate w/v, 37°C) was slowly added to cell

suspension and incubated for 20min at 37°C. Cells were pelleted at 400g and resuspended in 200µl residual supernatant. Cells were fixed with cold methanol/glacial acetic acid (3:1 vol/vol) 4C°. Cells were pelleted at 400g at 4°C and resuspended in 200µl residual supernatant. Fixation step was repeated 3 times. Fixed cells were dropped on glass slides to create Metaphase spreads. M-FISH was performed as described (20).

Human GCB cell culture

Fresh, tonsil tissue was sourced from the Addenbrooke's ENT Department, Cambridge with written informed consent of the patient/parent/guardian. Primary human GC B cells were isolated by MACS separation, cultured on CD40-L and IL-21 expressing YK-6 feeder cells and transduced as described before (21). Ethical approval for the use of human tissue was granted by the Health Research Authority Cambridgeshire Research Ethics Committee (REC no. 07/MRE05/44). At day 5 cells were transferred on CD40-L^{-}/IL-21^{-} feeder cells. Transduced (reporter^{+}) cells were counted by FACS using counting beads on day 5 and 12 post isolation.

Table A

	SOURCE	Catalogue number	Experiment
Brilliant Violet 421™ anti-mouse CD117 (c-Kit) Antibody	BioLegend	Cat#105828	FACS
APC anti-mouse CD117 (c-kit) Antibody	BioLegend	Cat#135108	FACS
Brilliant Violet 785™ anti-mouse Ly-6A/E (Sca-1) Antibody	BioLegend	Cat#108139	FACS
Biotin anti-mouse Ly-6G/Ly-6C (Gr-1) Antibody	BioLegend	Cat#108404	FACS
Biotin anti-mouse NK-1.1 Antibody	BioLegend	Cat#108704	FACS
Biotin anti-mouse CD11c Antibody	BioLegend	Cat#117303	FACS
Biotin anti-mouse/human CD11b Antibody	BioLegend	Cat#101203	FACS
Biotin anti-mouse TER-119/Erythroid Cells Antibody	BioLegend	Cat#116204	FACS
Biotin anti-mouse CD3ε Antibody	BioLegend	Cat#100303	FACS
BV785 anti-mouse B220 (Clone RA3-6B2)	BioLegend	Cat#103245	FACS
BV605 anti-mouse CD19 (Clone 6D5)	BioLegend	Cat#115539	FACS
BV785 anti-mouse CD19 (Clone 6D5)	BioLegend	Cat#115543	FACS
APC anti-mouse CD38	Biolegend	Cat#102711	FACS
APC anti-mouse/human CD45R/B220 Antibody	BioLegend	Cat#103212	FACS/Histology
Alexa Fluor® 647 Rat anti-Mouse CD267 - Clone 8F10 (RUO)	BD	Cat#558453	FACS

PE/Cy7 anti-mouse CD93 (AA4.1, early B lineage), Rat IgG2b, kappa	BioLegend	Cat#136506	FACS
APC anti-mouse CD93 (AA4.1, early B lineage),	BioLegend	Cat#136510	FACS
FITC Rat Anti-Mouse IgM Clone II/41 (RUO)	BD	Cat#553437	FACS
PE/Cy7 anti-mouse CD23, Rat IgG2a, kappa, Clone: B3B4	BioLegend	Cat#101614	FACS
PerCP/Cy5.5 anti-mouse IgD, Rat IgG2a, kappa, Clone: 11-26c.2a	BioLegend	Cat#405710	FACS
IgM Monoclonal Antibody (II/41), APC,	Ebioscience	Cat#17-5790-82	FACS
IgM Monoclonal Antibody (II/41), Biotin	Ebioscience	Cat#13 5790 81	FACS
IgD Monoclonal Antibody (11-26c (11-26)), Biotin	Ebioscience	Cat#13-5993-82	FACS
Biotin Rat Anti-Mouse Ig, κ Light Chain Clone 187.1 (RUO)	BD	Cat#559750	FACS
Biotin Rat Anti-Mouse Ig, λ1, λ2, & λ3 Light Chain Clone R26-46 (RUO)	BD	Cat#553433	FACS
Biotin Rat Anti-Mouse IgG1 Clone A85-1 (RUO)	BD	Cat#550331	FACS
Biotin Rat Anti-Mouse IgG2a/2b Clone R2-40 (RUO)	BD	Cat#553398	FACS
Biotin Rat Anti-Mouse IgG2a Clone R19-15 (RUO)	BD	Cat#553388	FACS
Biotin anti-mouse IgG3, immunoglobulin G3	BioLegend	Cat#406803	FACS
Biotin Rat Anti-Mouse IgE Clone R35-118 (RUO)	BD	Cat#553419	FACS
Anti-Mouse IgA Biotin	Ebioscience	Cat#13-5994-85	FACS
Streptavidin PE-Cyanine7 Conjugate	Ebioscience	Cat#25-4317-82	FACS
PE anti mouse CD138 (Syndecan-1), Rat IgG2a, kappa, Clone: 281-2	BioLegend	Cat#142504	FACS, histology
APC anti-mouse CD138 (Syndecan-1), Rat IgG2a, kappa, Clone: 281-2	BioLegend	Cat#142506	FACS
PE/Cy7 anti-human CD2, Mouse IgG1, kappa, Clone: TS1/8	BioLegend	Cat# 309214	FACS
APC anti-human CD2, Mouse IgG1, kappa, Clone: RPA-2.10	BioLegend	Cat#300213	FACS, histology
FITC anti-mouse CD21/CD35 (CR2/CR1), Rat IgG2a, kappa, Clone: 7E9	BioLegend	Cat#123407	FACS
PE Hamster Anti-Mouse CD95	BD	Cat#554258	FACS, histology
PE-Cy7 Hamster Anti-Mouse CD95	BD	Cat#557653	FACS
PE anti-mouse CD20 Antibody	BioLegend	Cat#150409	FACS
APC anti-mouse CD54 Antibody	BioLegend	Cat#116119	FACS

MHC Class II (I-A/I-E) Monoclonal Antibody (M5/114.15.2), PE,	eBioscience	Cat#12-5321-82	FACS
PE Rat Anti-Mouse Ig κ Light Chain	BD	Cat#562021	FACS
Human antibodies			
FITC anti-human CD19 Antibody	BioLegend	Cat#302256	FACS
APC anti-human HLA-DR, DP, DQ Antibody	BioLegend	Cat#61714	FACS
PE anti-human CD54 Antibody	BioLegend	Cat#353106	FACS
APC anti-human CD95 (Fas) Antibody	BioLegend	Cat#305612	FACS
FITC anti-human CD23 Antibody	BioLegend	Cat#338505	FACS
APC anti-human CD3 Antibody	BioLegend	Cat#300311	FACS
FITC anti-human CD20 Antibody	BioLegend	Cat#302304	FACS
APC/Cy7 anti-human Ig light chain κ Antibody	BioLegend	Cat#316522	FACS
PE anti-human Ig light chain lambda Antibody	BioLegend	Cat#316608	FACS
TruStain FcX™ (anti-mouse CD16/32, clone 93)	BioLegend	Cat#101320	FACS
Goat anti-MU Kappa (southern blot)	Southern bio	Cat#2050-01	elispot
Goat anti-MU Lambda (southern blot)	Southern bio	Cat#1060-01	elispot
Goat anti-MU Lambda Biotin (southern blot)	Southern bio	Cat#1060-08	elispot
Goat anti-MU Kappa Biotin (southern blot)	Southern bio	Cat#1050-08	elispot
Ha-Tag (C29F4) Rabbit mAb	Cell signaling	Cat#3724 P	Western blot ,IP, histology
c-Myc (D84C12) Rabbit mAb	Cell signaling	Cat#2278 S	Western blot
EBV LMP2A antibody [14B7] -	Abcam	Cat#ab59026	Western blot
MONOCLONAL ANTI-BETA ACTIN	Sigma	Cat#A2228-200UL	Western blot
XP RBPSUH (D10A4) XP Rabbit mAb	Cell signaling	Cat#5313 P	Western blot
Anti-LMP1 mouse hybridoma supernatant S12	Elliott Kieff Harvard medical school		Western blot
c-Rel-antibody	R&D systems	Cat# MAB2699	Western blot
goat anti-mouse IgG(H+L)-HRP	Dianova/ Jackson Dianova Immunoresearch	Cat#115-035-003	Western blot
Donkey anti-rabbit IgG (H+L)-HRP	Dianova/ Jackson Immunoresearch	Cat#711-035-152	Western blot
Donkey anti-rat IgG (H+L) - HRP	Dianova /Jackson Immunoresearch	Cat#712-035-150	Western blot
Goat Anti-Human IgD-BIOT	Southern Bio	Cat#2030-08	southern

Mouse Anti-Human CD44-BIOT	Southern Bio	Cat#9400-08	southern
BCL6 Antibody	Proteintech	Cat#21187-1-AP	histology
IRF4/Mum1 antibody	Proteintech	Cat#11247-2-AP	histology
CD10 antibody	St Johns laboratory	Cat#STJ97788	histology
c-Rel-antibody	R&D systems	Cat#AF2699-SP	histology
Rabbit Anti-Goat IgG(H+L)-FITC	Southern biotech	Cat# 6160-02	histology
Rat anti-Metallophilic Macroph.:Biotin, Clone MOMA 1, Isotype IgG2a	Dianova	Cat#T-2021	histology
Streptavidin, Rhodamine Red™-X conjugate	Thermo-fisher	Cat#S6366	histology
Goat Anti-Rabbit IgG(H+L), Mouse/Human ads-FITC	Southern biotech	Cat#4050-02	histology

Table B

Primers to amplify translocation sites in LMP1-Ls		
Chr11_Rnf145_rv	CCAAGGCTCGTGGATATTGT	
Chr12_Igh_rv	GCTGACTCCTGGTTGCTAGG	
Chr11_Rel_rv	CGCAGGAATGTGAGGAATGT	
Chr6_Igk_rv	AACACTGGATAAAGCAGTTTATGCCCTTTC	
Rosa26_fw	GGAGTGTTGCAATACCTTTCTGGGAGTTC	Control site
Rosa26_rv	TGTCCCTCCAATTTTACACCTGTTCAATTC	Control site
Primers to amplify CAS9 cutting sites		
Cdkn2a cr1+2+3_fw	GTCAGAAGCTTTTGGACCAACTA	
Cdkn2a cr1+2+3_rv	CGTACATAGGGCTTCTTTCTTGG	
B220_fw	CGGGAAGACTGTGAATAAGGAAC	
B220_rv	CATTCCACGTCCTGTTGTTTAGA	
Cd44_fw	AGTCTTCACTTACAAGCACTTCT	
Cd44_rv	TTCAACTGTCAGGGAGGAGCCTTCCAG	
Bcl2L11cr1-2-3_fw	CCTCCCTACAGACAGAACCG	
Bcl2L11cr1-2-3_rv	GGCTTTAAATGCTCCCCACA	
VDJ-PCR-Primers		
JH intronic REV	CTCCACCAGACCTCTCTAGACAGC	
VHA (J558/VH1)	ARGCCTGGGRCTTCAGTGAAG	
VHB (Q52/VH2)	CTCACAGAGCCTGTCCATCAC	
VHC (36-60/VH3)	TCTCAGWCTCTGTCYCTCACC	
VHE (7183/VH5)	GTGGAGTCTGGGGGAGGCTTA	
VHF (J606/VH6, S107/VH7, X24/VH5)	WCTGGAGGAGGCTTGGTGCAA	
VHG (GAM3/VH9)	GGAGAGACAGTCAAGATCTCC	
sgRNA sequences		
B220	CAGTGGTGCGAGCAGGTAAG	
Bcl2l11 #1	GTGCACTGAGATAGTGGTTGA	
Bcl2l11 #2	GTTGACTTGTCACAACTCAT	
Bcl2l11#3	GTACCCATTGCACTGAGATAG	

Cd44	CTACGCAGGTGTATTCCATG	
Cdkn2a #1	CCCCACTACCTTCTCCCGCC	
Cdkn2a #2	GTCGTGCACCGGGCGGGAGA	
Cdkn2a #3	GCGGTGCAGATTCGAACTGCG	
LMP1 #1	T TAA TCT GGA TGT ATT ACC A	
LMP1 #2	C CAA AAC AGT AGC GCC AAG	
LMP1 #3	A ATC ATC GGT AGC TTG TTG	
unspecific*	ACTCCAGTCTTTCTAGAAGA	*recognizes sequence in Rose26 which is absent in R26LMP1^{stopf}/R26Cas9^{tg} mice
RT-qPCR primers		
Arf-fw	TGTTGAGGCTAGAGAGGATCTTG	
Arf-rv	CTGCACCGTAGTTGAGCAGA	
Bcl2l11-fw	GAGATACGGATTGCACAGGA	
Bcl2l11-rv	TCAGCCTCGCGGTAATCATT	
Hprt-fw	GTCATGCCGACCCGCAGTC	
Hprt-rev	GTCCTGTCCATAATCAGTCCATGAGGAATAAAC	
Ink4A-fw	CGACGGGCATAGCTTCAG	
Ink4A-rv	GCTCTGCTCTTGGGATTGG	
Myc-fw	GCCAGCCCTGAGCCCCTAGT	
Myc-rv	AGCAAACCTCCGCACAGCCC	
Prdm1-fw	CCAGGTCTGCCACAAGAGATT	
Prdm1-rv	TCCGATGACTCATAGAGGCTG	

Supplemental figures

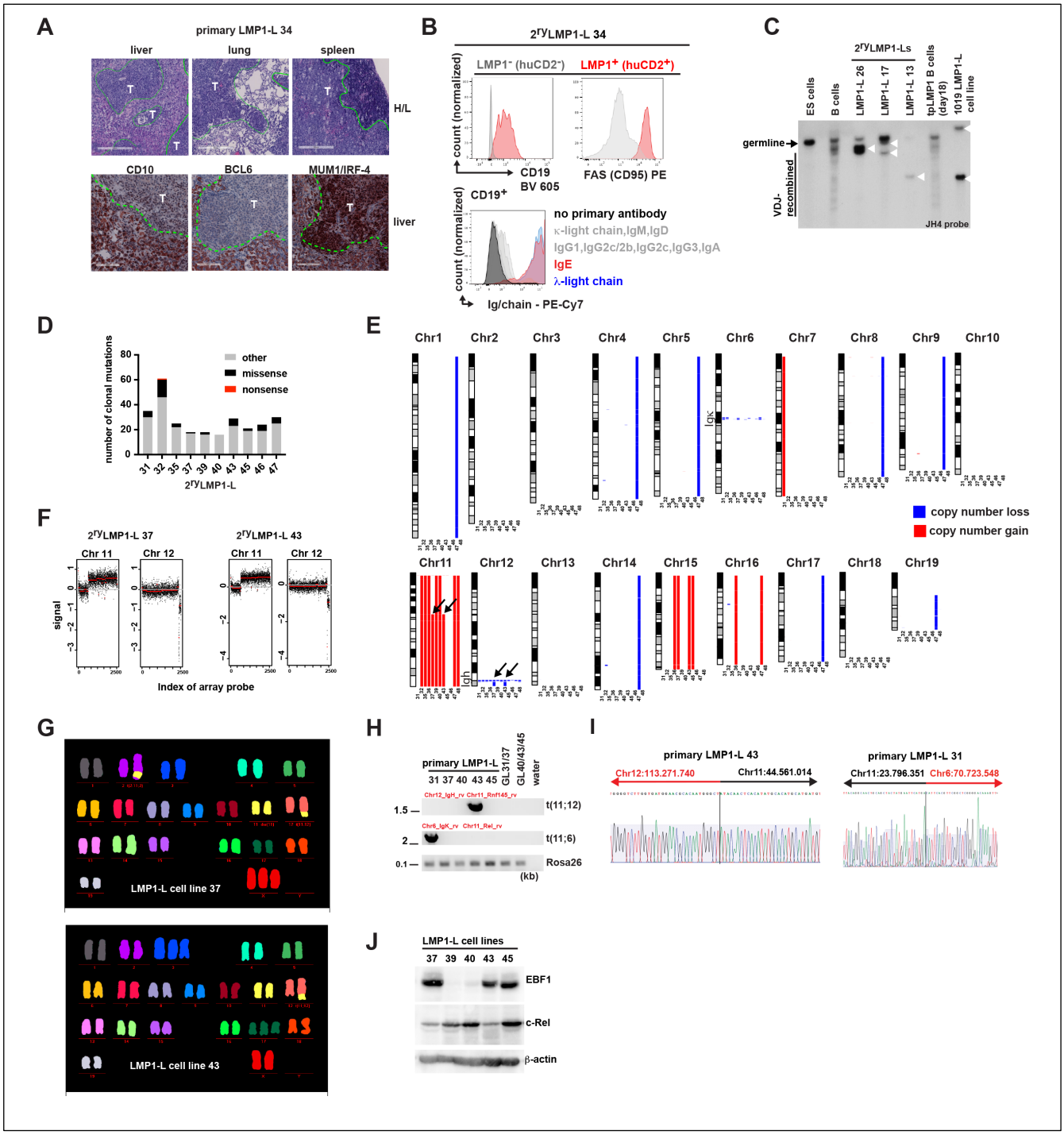

Figure S1 Characterization of LMP1-Ls

A Histological sections of primary LMP1-L 34 (representative of 13 analyzed tumors). Upper panel: representative Hämalaun (H/L) staining. Lower panel: immuno-histology staining. Tumor (T) outlines are indicated in green. Scale Bars indicate 300μm (upper panel) and 100μm (lower panel). **B** Representative FACS-analysis of surface markers of 2^{ry}LMP1-L 34. Left panel: Expression of B cell marker (CD19) and LMP1 target gene (FAS) on LMP1^{+} (huCD2^{+}) (red) and LMP1^{-} (huCD2^{-}) cells (grey). Right Panel: Ig-light and -heavy chain surface expression on CD19^{+} cells **C** Southern blot for VDJ-rearrangements in 2^{ry}LMP1-Ls. As controls, C57BL/6 Embryonic Stem cells (ES-cells), CD43^{-} C57BL/6 B cells, tpLMP1 B cells and a previously established LMP1-L cell line 1019 are presented. White arrow heads indicate clonal VDJ-arrangements **D** Full exome sequencing of sorted (huCD2^{+}) 2^{ry}LMP1-Ls. Absolute number of exome mutations in LMP1-Ls with a read-frequency of more than 35% (considered as clonal) is presented. Other mutations include silent mutations, mutations in non-coding sequences and mutations in non-protein-coding transcripts. (all clonal mutations are listed in Table S2) **E** Array-CGH detecting copy number changes in 2^{ry}LMP1-L. Arrows indicate shared copy number variations (CNVs) between tumors 37 and 43. (all CNVs are listed in table S3) **F** Detailed analysis of copy number changes in Chr11 and 12 in Array-CGH **G** Representative M-

FISH on LMP1-L cell lines 37 and 43 (M-FISH analysis is summarized in table S4) **H** PCR on gDNA of primary LMP1-Ls or germline (GL) gDNA. Amplicons are spanning predicted translocation sites in LMP1-Ls 31 (t11;6) and 43 (t11;12). (Ig translations predicted by exome sequencing are listed in table S5). PCR amplifying a Rosa26-fragment is presented as a loading control **I** Sanger sequencing of chimeric PCR products from (H) **J** Western blot of total cell lysates from LMP1-CLs

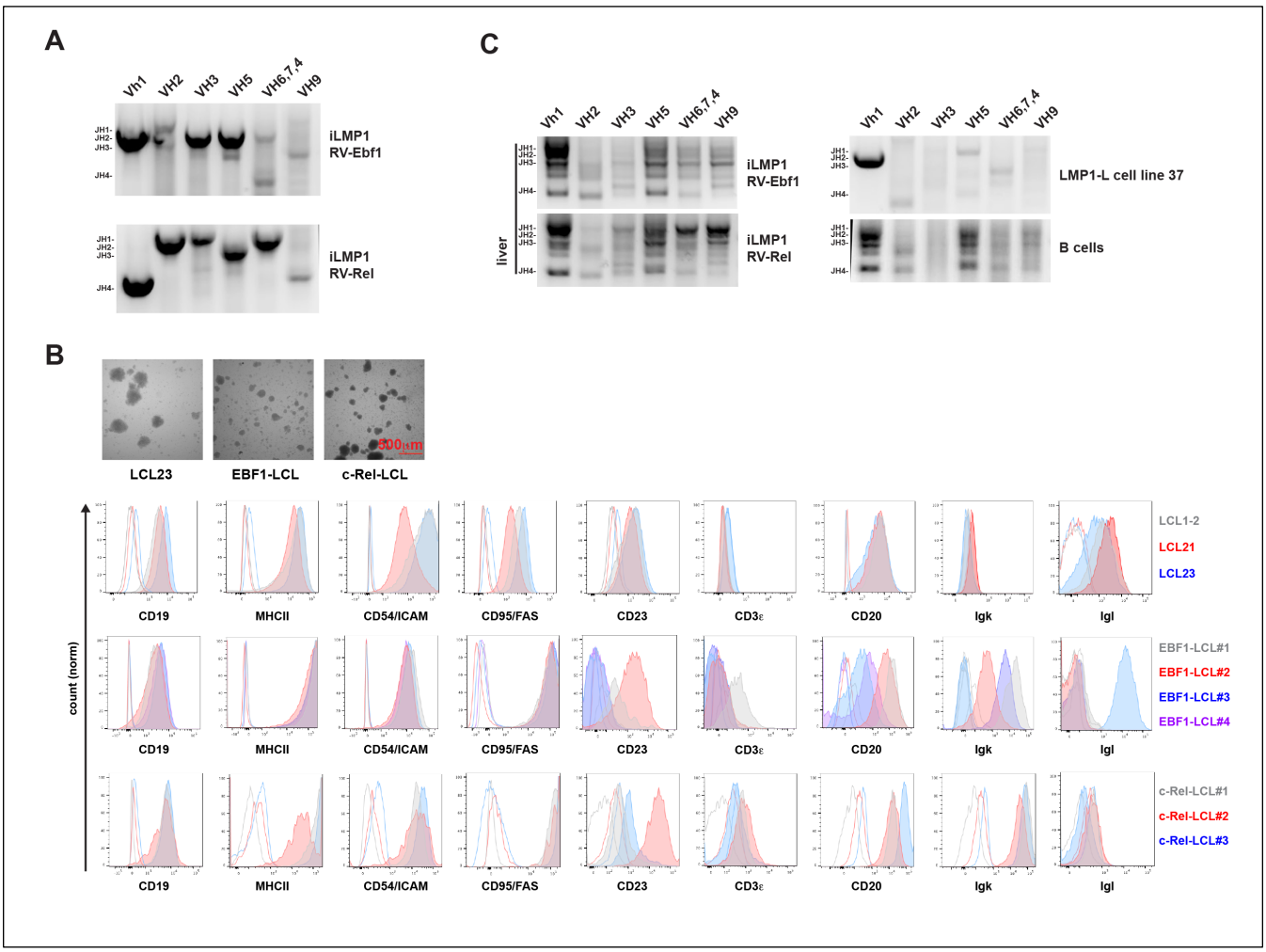

Figure S2 Characterization of LMP1/EBF1 and LMP1/c-Rel expressing B cells

A VDJ-PCR on bulk populations of iLMP1 B cells 45 days post transduction with RVs encoding *Ebf1-ires-GFP* or *Rel-ires-GFP* (from Fig. 2B). JH1-4 indicate approximate sizes of amplicons involving respective JH segments. **B-C** Phenotyping of EBF1- and c-Rel-LCLs (4-5 month of culture). **B** White light images of cultured cells. **C** FACS-analysis of common LCL surface molecules. Non-filled histograms depict respective unstained controls. Human LCLs 21, 23 and 12 are presented as controls. **D** VDJ-PCR on *Ebf1*- or *Rel*-transduced iLMP1 B cells expanding in $RAG2^{KO}c\gamma^{KO}$ mice transplanted with $3*10^5$ reporter$^+$ cells (from Fig. 2D). Analysis was performed on liver gDNA at disease onset. LMP1-L cell lines 37 and splenic CD43$^-$ C57BL/6 B cells serve controls for clonal and polyclonal populations, respectively.

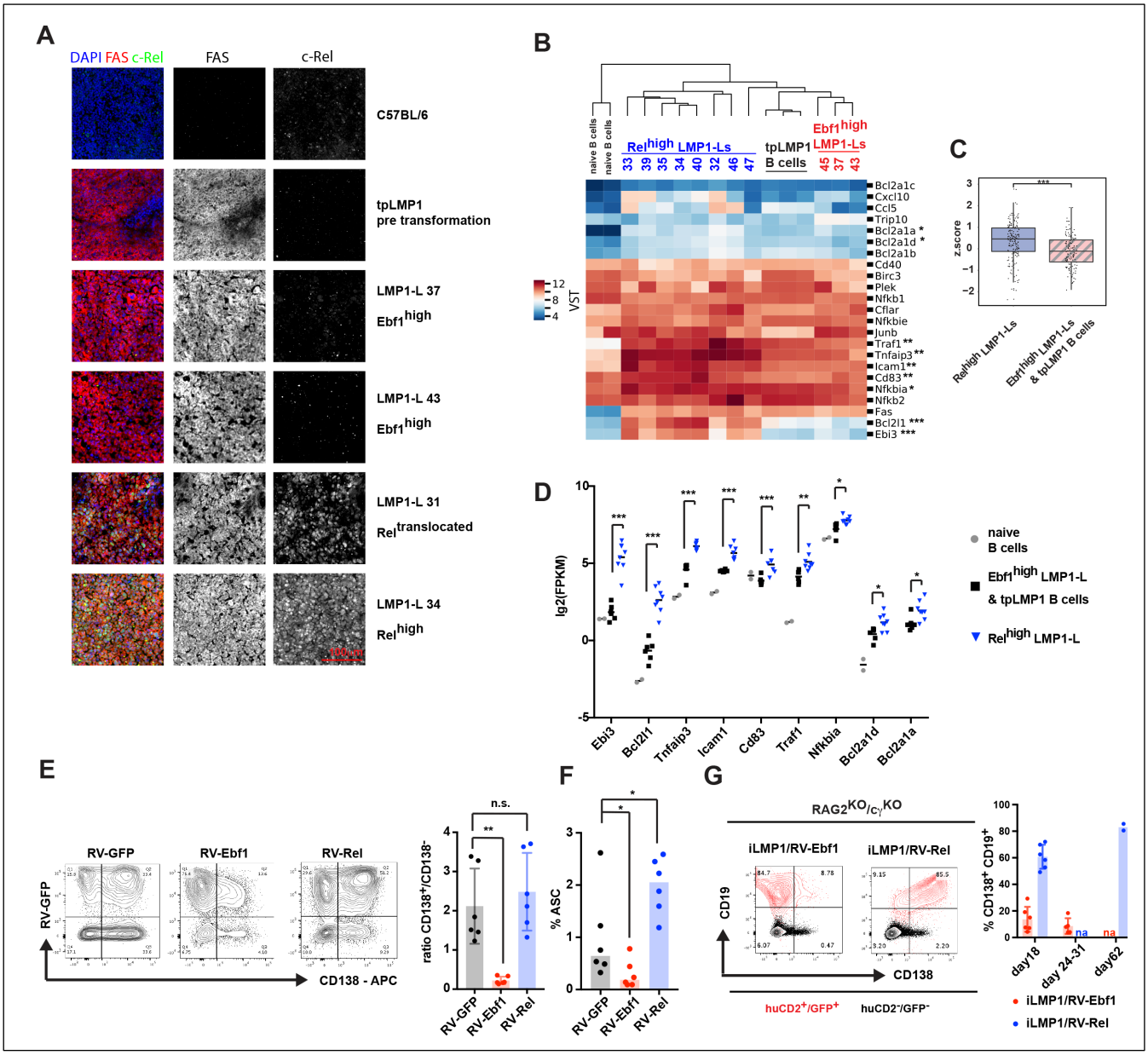

Figure S3 Characterization of EBF1 and c-Rel activity in LMP1 B cells

A Representative immuno-histology on splenic sections of 2nd LMP1-Ls. Sections from spleens of C57BL/6 and tpLMP1 mice are shown as control. FAS serves as a surrogate marker for LMP1 expression (huCD2 could not be detected in PFA-fixed sections). (tpLMP1 is representative for 3 cases analyzed; LMP1-Ls 34 is representative for 6 Rel^{high} cases analyzed) **B-D** Further analysis of RNA-sequencing of LMP1-Ls and tpLMP1 B cells from (Fig. 1E) **A** Non-supervised clustering (Euclidean distance and average linkage) performed on VSD-normalized expression data of established LMP1/NF-κB target genes in LMP1-Ls. **B** Z-score normalized expression of all LMP1/NF-κB target genes. Each dot represents expression level of 1 gene in 1 LMP1-L or tpLMP1 B cell sample. **C** FPKM-normalized expression of LMP1/NF-κB target genes with significantly altered expression in *Rel*^{high} LMP1-Ls compared to *Ebf1*^{high} LMP1-Ls and tpLMP1 B cells **E-F** $CD43^-$ Splenic B cells from C57BL/6 mice were stimulated with αCD40 (2μg/ml) and IL-4 (20ng/ml). At 24h cells were transduced with RVs encoding, *Ebf1*-ires-GFP or *Rel*-ires-GFP. At 48h cells were transferred to 40LB feeders in the presence of IL-21 (20ng/ml). **E** Representative FACS-blots and quantification showing the ratio of $CD138^+$ over $CD138^-$ $reporter^+$ cells on day 11 post stimulation; n=6. **F** Quantification of Elispot-assays for total (κ/λ)-antibody secreting cells in FACS-sorted $reporter^+$ cells; n=6. Bars indicate median frequency **G** Further analysis of RV-transduced iLMP1 B cells transplanted into *RAG2*^{KO}*c*γ^{KO} mice (from experiment 2 D-G). Representative FACS-blots and quantification of PB-differentiation are presented (day 18 n=6 (not shown in Figure 2); *Ebf1* day 24-31 n=5; *Rel* day 62 n=2). Unless noted data are presented as mean ± SD. Significance was calculated using a Student's t-test, p value adjusted via Benjamini & Hochberg (A), student t-test (B,C), one-way Anova with P-value adjusted via Dunnett (G) or paired students t-test (F) (*p<0.05; **p<0.005; ***p< 0.0005; n.s. non-significant)

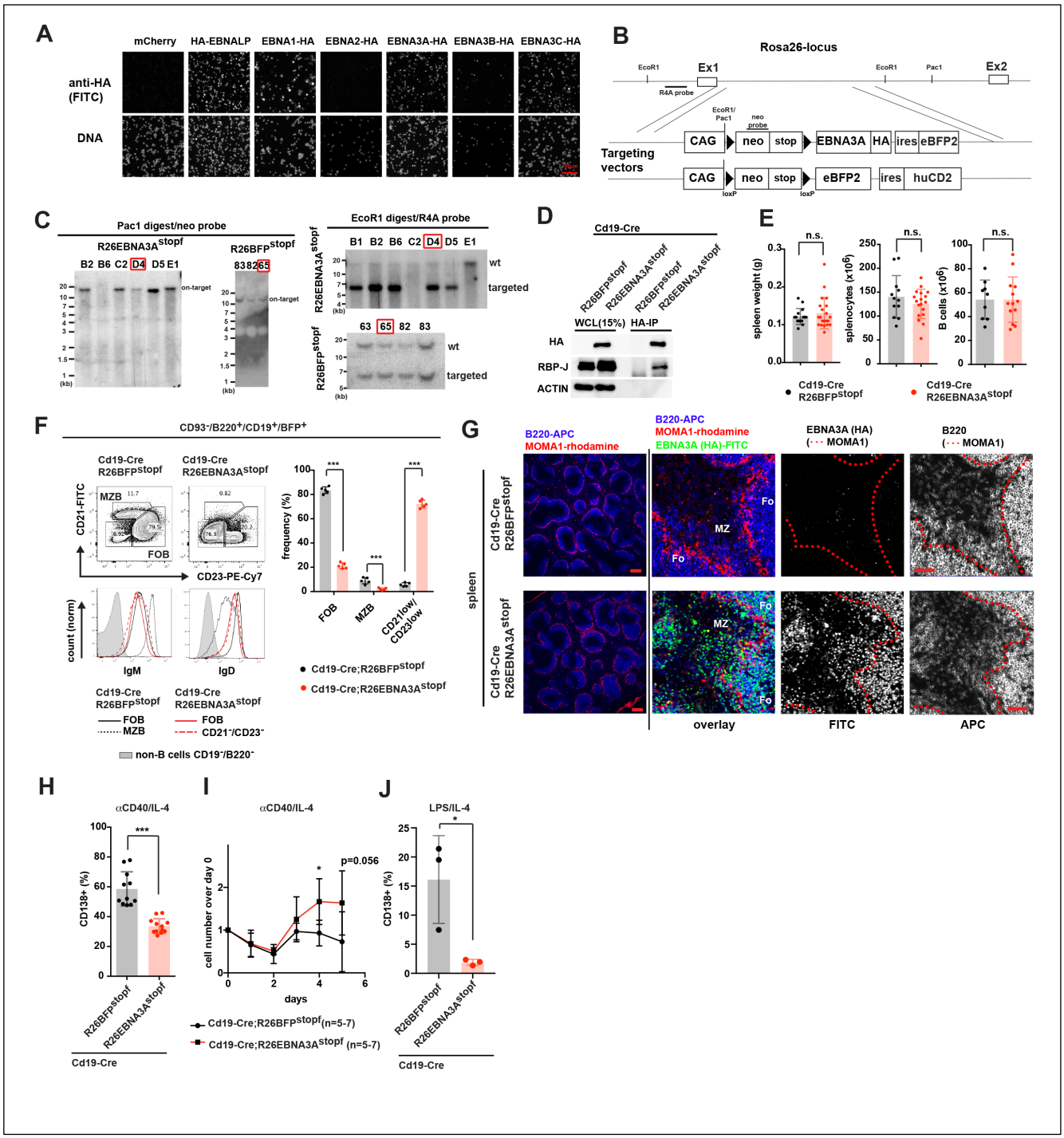

Figure S4 Characterization of EBNA3A expression in mouse B cells

A Immunofluorescence of sorted mCherry^{+} iLMP1 B cells transduced with RVs encoding mCherry or HA-tagged EBNA-ORFs on detecting the HA-TAG on day 4 post TAT-Cre **B** Targeting strategy for *R26EBNA3A^{stopf}* and *R26BFP^{stopf}* alleles. CAG: artificial promotor; neo: neomycin resistance gene; stop: transcriptional stop cassette; HA: Human influenza hemagglutinin-TAG; loxP: recombination site for Cre-recombinase; huCD2: cytoplasmic signaling domain deleted human CD2; ires: internal ribosome entry site. Restriction enzyme digest cutting sites and probes for southern blot are indicated. **C** Southern blot of indicated ES-cell clones, detecting on-target integration (R4A probe) and potential random integrations (neo-probe). Clone D4 was selected to create the *R26EBNA3A^{stopf}* line. Clone 65 was selected to create the *R26BFP^{stopf}* line **D-I** Analysis of Cd19-Cre R26EBNA3A^{stopf} and *Cd19-Cre;R26BFP^{stopf}* mice **D** Western Blot of whole cell lysate (WCL) or HA-co-immunoprecipitation performed with lysates of αCD40 (2μg/ml) and IL-4 (20ng/ml) stimulated splenic B cells from indicated genotypes on day 4. (Representative of 2 experiments) **E** Quantifications showing spleen weight, total splenic cell number and total splenic B cell number (CD19^{+}/B220^{+}); spleen size n=15 (Cd19-Cre;R26BFP^{stopf}), n=21 (Cd19-Cre;R26EBNA3A^{stopf}); splenocytes: n=12 (Cd19-Cre;R26BFP^{stopf}), n=18 (Cd19-Cre; R26EBNA3A^{stopf}); B cells: n=9 (Cd19-Cre R26BFP^{stopf}), n=13 (Cd19-Cre R26EBNA3A^{stopf}) **F** Representative FACS-analysis of

$BFP^+/CD93^-/CD19^+/B220^+$ mature splenic B cells. Upper panels and quantification show frequency of $CD23^{low}CD21^+$ marginal zone B cells (MZB), $CD23^+CD21^{low}$ Follicular B cells (FOB) and $CD23^{low}CD21^{low}$ cells; n=5. Lower histograms depict IgM and IgD expression in indicated subgroups (representative of 5 biological replicates). Non-B cells are presented as low control **G** Immuno-histology on splenic sections representative of 4 independent mice per group. Red dotted lines indicate the follicle-boarder (MOMA-1 staining). Fo (Follicle) MZ (Marginal zone) **H-J** Analysis of FACS-sorted reporter$^+$ $CD19^+/CD23^+$ FOBs. **H** FOBs were stimulated in vitro with αCD40 (2μg/ml) and IL-4 (20ng/ml) for 2 days then transferred on 40LB feeder cells in the presence of IL-21 (20ng/ml). Quantification shows CD138 expression among reporter$^+$ cells on day 11 (aCD40/IL-4); n=11 (Cd19-Cre;$R26BFP^{stopf}$), n=12 (Cd19-Cre;$R26EBNA3A^{stopf}$). **I** In vitro growth curve of FACS-sorted $BFP^+/CD19^+/CD23^+$ FOBs stimulated with αCD40 (2μg/ml) and IL-4 (20ng/ml); n=8 (day 0,1,2,3,4) n=6 (day5). **J** FOBs were stimulated with LPS (10μg/ml) and IL-4 (20ng/ml). Quantification shows CD138 expression among reporter$^+$ cells on day 5; n=3.

Data are presented as mean ± SD. Significance was calculated using a non-paired Student's t-test (E,H,I,J) or two-way Anova with Sidak's multiple comparisons test (F) (*$p<0.05$; **$p<0.005$; ***$p<0.0005$; n.s. non-significant)

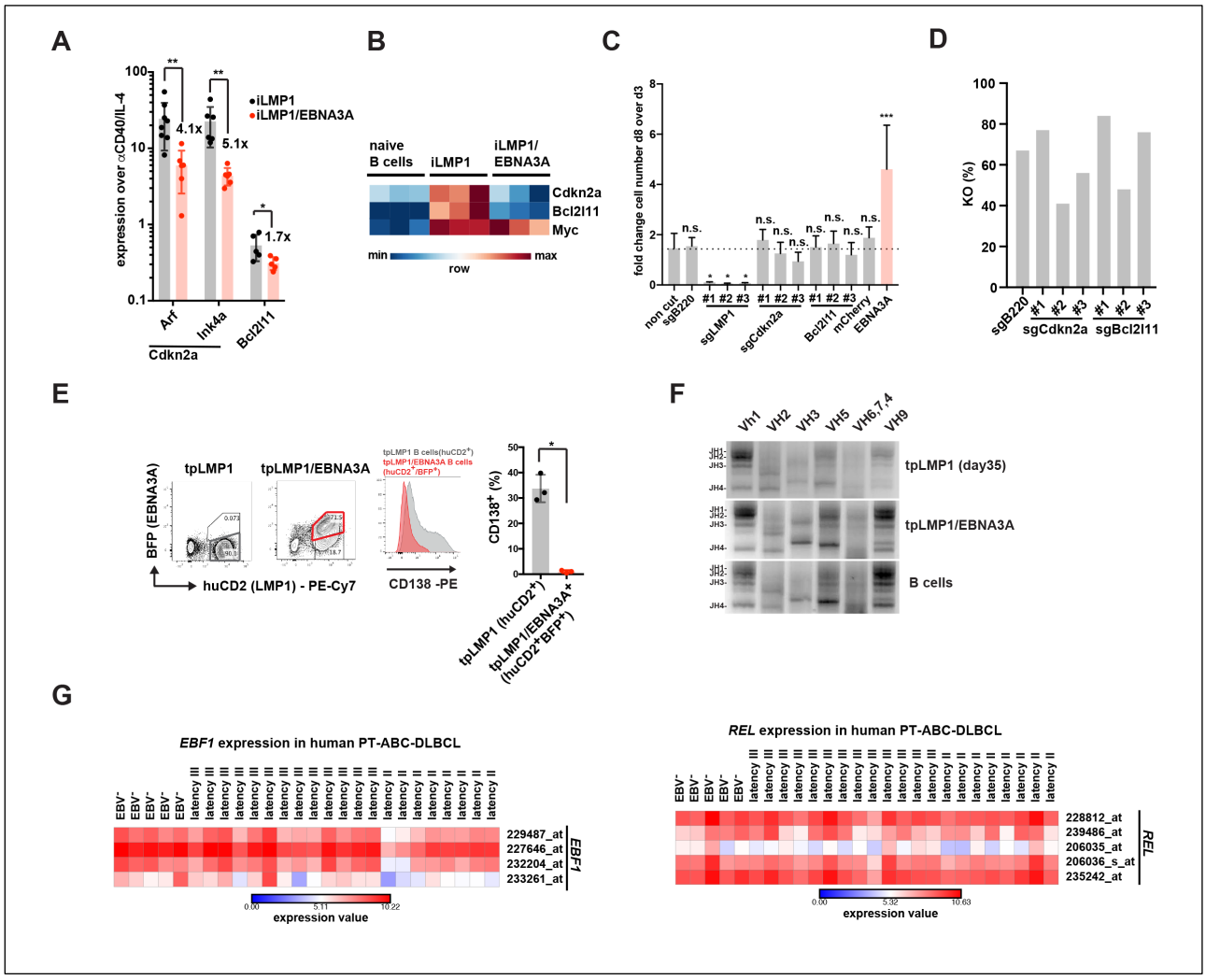

Figure S5 Characterization of LMP1/EBNA3A B cells

A RT-qPCR-based quantification of *Arf*-, *Ink4a*- and *Bcl2l11*-expression in iLMP1 and iLMP1/EBNA3A B cells day 6 post TAT-Cre. Expression is normalized to HPRT and the expression levels of CD43$^-$ naïve splenic B cells stimulated with αCD40 (2μg/ml) and IL-4 (20ng/ml) for 4 days. Fold change is indicated; n=8 (iLMP1;*Arf*); n=6 (iLMP1/EBNA3A;*Arf*); n=6 (*Ink4a*); n=5 (*Bcl2l11*) **B** Heatmap showing lg2-FPKM-normalized expression of indicated genes in RNA-sequencing from Fig. 5D **C-D** CD43$^-$ B cells from *R26LMP1^{stopf}/CAS9^{tg}* were treated with TAT-Cre (iLMP1/CAS9). iLMP1/CAS9 B cells were either transduced with RVs encoding mCherry, EBNA3A-ires-mCherry or sgRNAs targeting indicated genes (reported by mCherry or BFP). B220- and LMP1-guides were used as a non-selected and negatively selected knockout control, respectively **C** Quantification of reporter$^+$ cell number day 8 over day 3 is presented. *Cdkn2a*-gRNAs target *Ink4a*- and *Arf*-ORF; n=5 **D** KO-efficiency in sorted reporter$^+$ cells on day 6 post TAT-Cre as estimated by ICE-analysis. **E-F** Analysis of tpLMP1 and tpLMP1/EBNA3A mice (from Fig. 5E) **E** Representative FACS-analysis and quantification of reporter$^+$CD138$^+$ PBs in spleens on day 35 p.t.; n=3 **F** VDJ-PCR on splenic cells at day 35 p.t.. CD43$^-$ splenic C57BL/6 B cells serve as a positive control for a polyclonal B cell population (representative of 3 biological replicates). **G** Reanalyzes of a CHIP-array from Morscio et al showing *REL* and *EBF1* expression in human PT-ABC-DLBCL. Rows represent independent probes on the array. Data are presented as mean ± SD. Significance was calculated using a Man-Whitney U test (A), one-way Anova with P-value adjusted via Dunnett (C) or Welch's t-test (E) (*p<0.05; **p<0.005; ***p< 0.0005; n.s. non-significant)

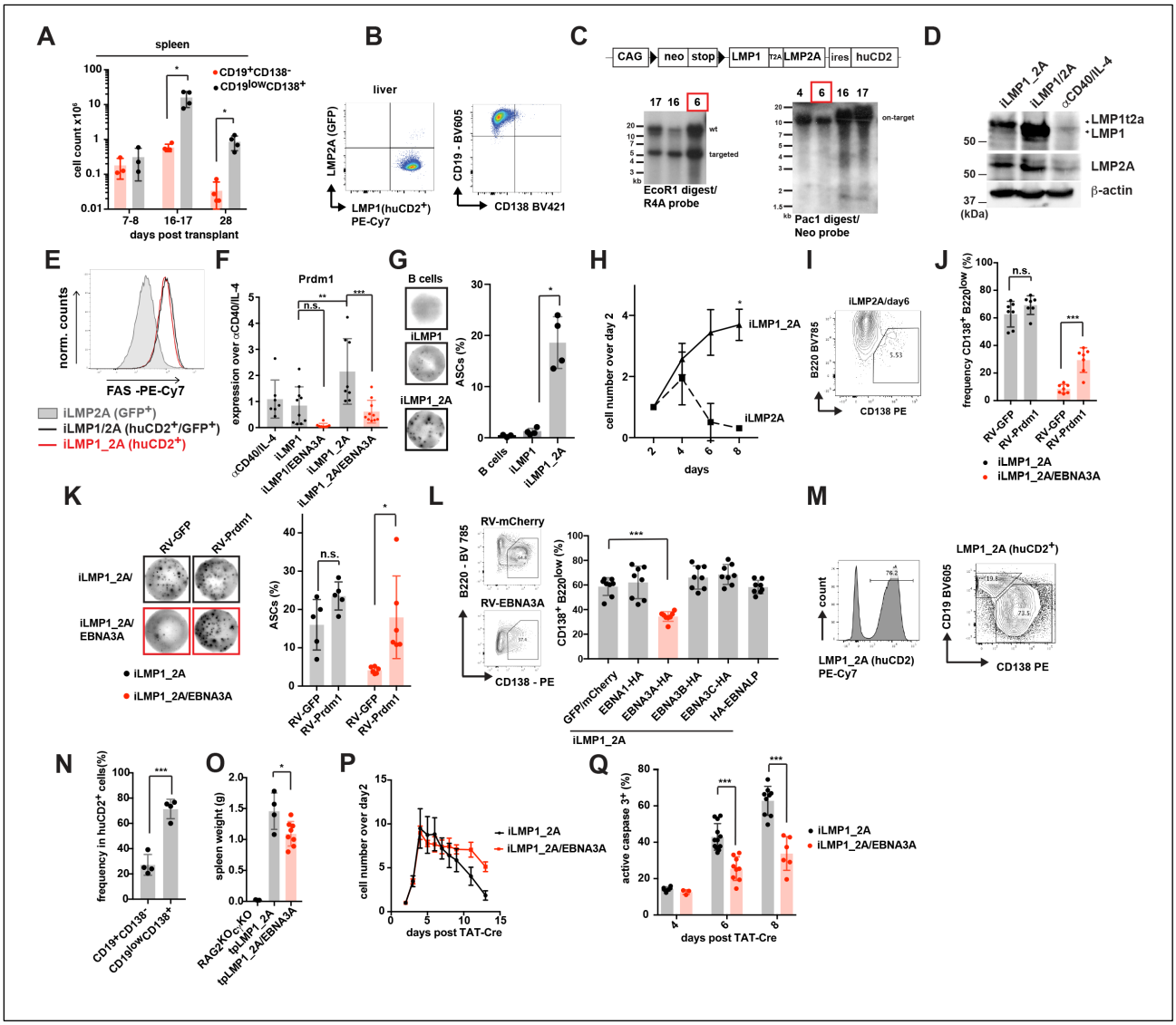

Figure S6 Characterization of LMP1, LMP2A and EBNA3A co-expressing B cells

A 3*10^6 B cells from Cγ1-Cre R26LMP1^{stopf}/R26LMP2A^{stopf} were transferred into RAG2^{KO} mice (see also Fig. 6A). Quantification shows absolute number of splenic huCD2$^+$/GFP$^+$ B cells (CD19$^+$/CD138$^-$) or PCs (CD138$^+$/CD19^{low}) at indicated timepoints after reconstitution; n=3 (day7-8), n=4 (day16-17/28) **B** CD19$^+$CD138$^-$huCD2$^+$GFP$^-$ LMP1-Lymphoma arising in one mouse of (A) **C** Southern blot of indicated ES-cell clones, detecting on-target integration (R4A-probe) and additional random integrations (neo-probe). Clone 6 was selected to generate the *R26LMP1_LMP2A^{stopf}* line. Targeting strategy for the *R26LMP1_LMP2A^{stopf}* allele is indicated. neo: neomycin resistance gene; stop: transcriptional stop cassette; loxP: recombination site for Cre-recombinase; huCD2: cytoplasmic signaling domain deleted human CD2; ires: internal ribosome entry site **D** Western blot of whole cell lysates from iLMP1_LMP2A and iLMP1/LMP2A B cells day 4 post TAT-Cre. Wild type B cells stimulated for 4 days with αCD40 (2μg/ml) and IL-4 (20ng/ml) serve a negative control for LMP1 and LMP2A expression. (representative of 2 experiments) **E** Representative FACS-analysis of iLMP1_LMP2A and iLMP1/LMP2A B for expression of LMP1-target gene FAS on day 3 post TAT-Cre (representative of 2 biological replicates). iLMP2A B cells are presented as a low control **F** RT-qPCR-based quantification of *Prdm1*-expression in sorted reporter$^+$ cells day 6 post TAT-Cre. Expression was normalized to HPRT and CD43$^-$ splenic C57BL/6 B cells stimulated with αCD40 (2μg/ml) and IL-4 (20ng/ml) for 4 days. n=7 (CD40/IL-4); n=10 (iLMP1 and iLMP1_2A/EBNA3A), n=8 (iLMP1/EBNA3A and iLMP1_2A) **G** Elispot for total (κ/λ) antibody secreting cells on sorted reporter$^+$ cells day 9 post TAT-Cre treatment or non-stimulated CD43$^-$ splenic C57BL/6 B cells taken ex vivo. Quantification and images of representative images of wells with 93 cells are presented; n=3 (B cells), n=4 (iLMP1 and iLMP1_2A) **H** Growth curve of bulk cultures; n=3 **I** FACS-analysis for PC marker expression on iLMP2A B cells on day 6 post TAT-Cre (Representative of 2 biological replicates) **J-K** iLMP1_LMP2A and iLMP1_LMP2A/EBNA3A B cells were transduced with RVs encoding GFP or *Prdm1*-ires-GFP and analyzed on day 9 post TAT-Cre **J** FACS-based

quantification of $CD138^+/B220^{low}$ plasma cells; n=7 **K** Elispot for total (κ/λ)-antibody secreting cells in FACS-sorted reporter$^+$ iLMP1_LMP2A and iLMP1_LMP2A/EBNA3A B cells transduced with RVs encoding GFP or *Prdm1*-ires-GFP. Quantification and representative images of wells with 120 cells are presented. n=5 (LMP1_2A), n=6 (LMP1_2A/EBNA3A) **L** Quantification of $CD138^+/B220^{low}$ plasma cells among reporter$^+$ LMP1_2A B cells transduced with RVs encoding mCherry, GFP or HA-tagged EBNA genes (reported by ires-mCherry or GFP) on day 9 post TAT-Cre; n=8 **M** Representative FACS-analysis of CD138 and CD19 expression on $huCD2^+$ cells in spleens of tpLMP1_2A mice at disease onset **N** Quantification of **(m)**; n=4 **O** Quantification of spleen size in tpLMP1_2A and tpLMP1_2A/EBNA3A mice at disease onset; n=3 ($RAG2^{KO}c\gamma^{KO)}$,n=4 (tpLMP1_2A), n=8 (tpLMP1/EBNA3A) **P** Growth curve of bulk culture; n=6 (iLMP1/LMP2A), n=3 (iLMP1_LMP2A/EBNA3A). **Q** FACS-based quantification of active caspase 3; n=6 (LMP1_2A day4), n=3 (LMP1_2A/EBNA3A day4), n=9 (LMP1_2A day6), n=9 (LMP1_2A/EBNA3A day6), n=6 (LMP1_2A day8), n=6 (LMP1_2A/EBNA3A day8). Data are presented as mean ± SD. Significance was calculated using a Welch's t-test (A, H), Man-Whitney U test (G), one-way Anova with P-value adjusted via Dunnett (F) non-paired Student's t-test (N,O,Q) or a paired Student's t-test (J, K, L) (*p<0.05; **p<0.005; ***p< 0.0005; n.s. non-significant)

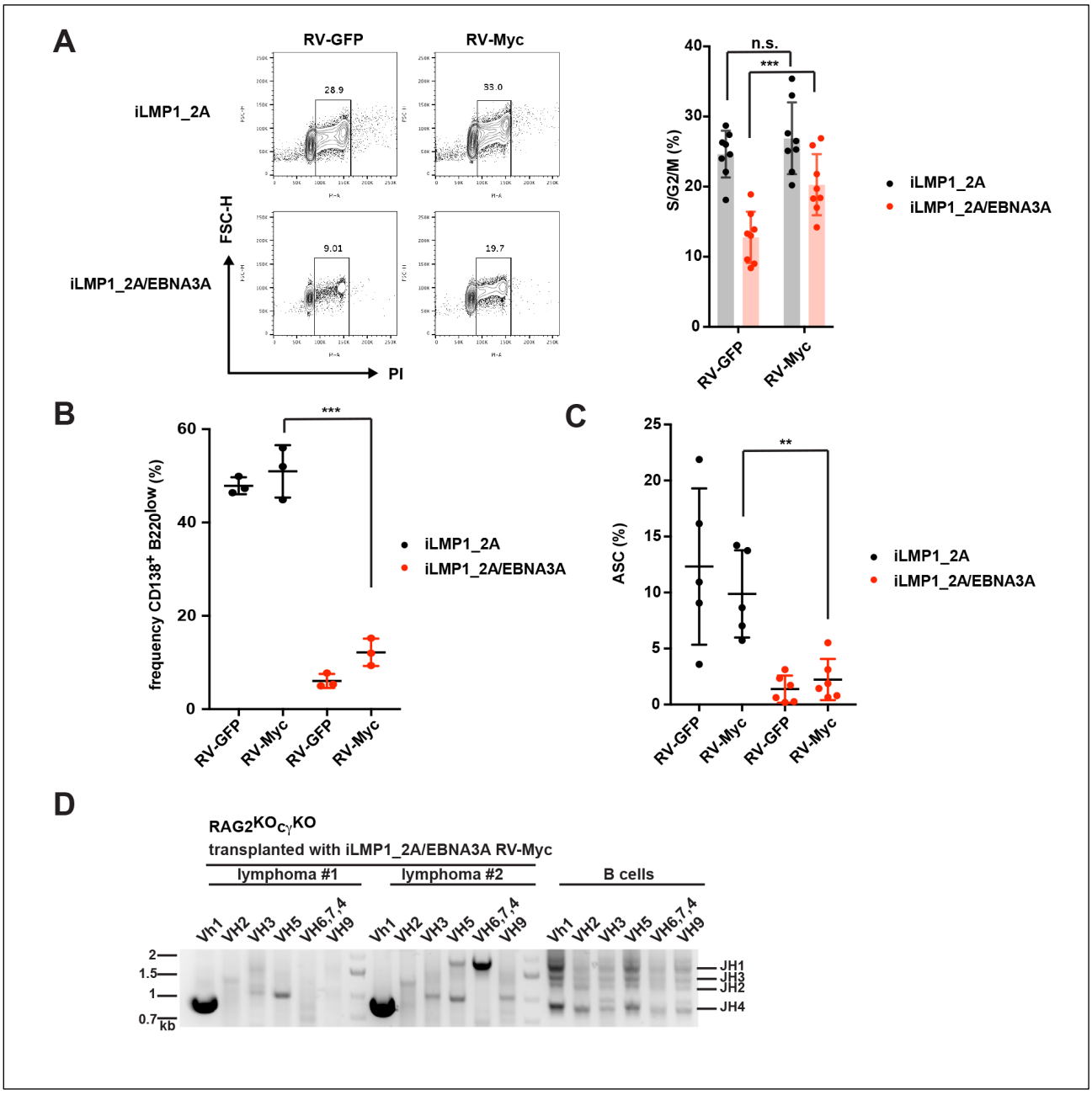

Figure S7 The role of Myc in LMP1, LMP2A and EBNA3A co-expressing B cells
iLMP1/LMP2A and iLMP1_LMP2A/EBNA3A B cells transduced with RVs encoding GFP or *Myc*-ires-mCherry **A** Representative FACS-analysis and quantification of sorted reporter$^+$ cells in S/G2/M phase on day 6; n=8 **B** FACS-based quantification of CD138$^+$B220low PCs on day 9; n=3. **C** Quantification of Elispot-assays for total (κ/λ)-antibody secreting cells in FACS-sorted reporter$^+$ cells on day 9; n=5 (iLMP1_2A) n=6 (iLMP1_2A/EBNA3A). **D** VDJ-PCR of two lymphomas arising in *RAG2^{KO}cγ^{KO}* mice transferred with 5*10^6 *Myc*-transduced iLMP1_2A/EBNA3A B cells on day 3 after TAT-Cre (from Fig. 7G). CD43$^-$ splenic B cells of C57BL/6 mice were used as a positive control for a polyclonal B cell population. Data are presented as mean ± SD. Significance was calculated using a paired Student's t-test (A), Student's t-test (B) or Welch's test (C) (*p<0.05; **p<0.005; ***p< 0.0005; n.s. non-significant)

1. T. Nojima, *et al.*, In-vitro derived germinal centre B cells differentially generate memory B or plasma cells in vivo. *Nat. Commun.* **2**, 465 (2011).
2. S. Sander, *et al.*, Synergy between PI3K Signaling and MYC in Burkitt Lymphomagenesis. *Cancer Cell* **22**, 167–179 (2012).
3. D. A. Conner, Mouse Embryo Fibroblast (MEF) Feeder Cell Preparation. *Curr. Protoc. Mol. Biol.* **51**, 23.2.1-23.2.7 (2000).
4. M. Peitz, K. Pfannkuche, K. Rajewsky, F. Edenhofer, Ability of the hydrophobic FGF and basic TAT peptides to promote cellular uptake of recombinant Cre recombinase: A tool for efficient genetic engineering of mammalian genomes. *Proc. Natl. Acad. Sci.* **99**, 4489–94 (2002).
5. T. Hsiau, *et al.*, Inference of CRISPR Edits from Sanger Trace Data. *bioRxiv*, 251082 (2019).
6. C. M. Wilke, *et al.*, A genomic copy number signature predicts radiation exposure in post-Chernobyl breast cancer. *Int. J. Cancer* **143**, 1505–1515 (2018).
7. H. Li, Aligning sequence reads, clone sequences and assembly contigs with BWA-MEM. *arXiv:1303.3997v2* (2013) (August 12, 2019).
8. K. Cibulskis, *et al.*, Sensitive detection of somatic point mutations in impure and heterogeneous cancer samples. *Nat. Biotechnol.* **31**, 213–9 (2013).
9. W. McLaren, *et al.*, The Ensembl Variant Effect Predictor. *Genome Biol.* **17**, 122 (2016).
10. A. M. Newman, *et al.*, FACTERA: a practical method for the discovery of genomic rearrangements at breakpoint resolution. *Bioinformatics* **30**, 3390–3 (2014).
11. R. Wurmus, *et al.*, PiGx: reproducible genomics analysis pipelines with GNU Guix. *Gigascience* **7** (2018).
12. S. Anders, W. Huber, Differential expression analysis for sequence count data. *Genome Biol.* **11** (2010).
13. M. I. Love, W. Huber, S. Anders, Moderated estimation of fold change and dispersion for RNA-seq data with DESeq2. *Genome Biol.* **15**, 550 (2014).
14. W. Shi, *et al.*, Transcriptional profiling of mouse B cell terminal differentiation defines a signature for antibody-secreting plasma cells. *Nat. Immunol.* **16**, 663–673 (2015).
15. E. D. Cahir-McFarland, *et al.*, Role of NF-kappa B in cell survival and transcription of latent membrane protein 1-expressing or Epstein-Barr virus latency III-infected cells. *J. Virol.* **78**, 4108 (2004).
16. W. S. Pear, *et al.*, Efficient and rapid induction of a chronic myelogenous leukemia-like myeloproliferative disease in mice receiving P210 bcr/abl-transduced bone marrow. *Blood* **92**, 3780–92 (1998).
17. V. T. Chu, *et al.*, Efficient CRISPR-mediated mutagenesis in primary immune cells using CrispRGold and a C57BL/6 Cas9 transgenic mouse line. *Proc. Natl. Acad. Sci.* **113**, 12514–12519 (2016).
18. T. Wirtz, *et al.*, Mouse model for acute Epstein-Barr virus infection. *Proc. Natl. Acad. Sci. U. S. A.* **113**, 13821–13826 (2016).
19. V. T. Chu, *et al.*, Efficient generation of Rosa26 knock-in mice using CRISPR/Cas9 in C57BL/6 zygotes. *BMC Biotechnol.* **16**, 4 (2016).
20. J. B. Geigl, S. Uhrig, M. R. Speicher, Multiplex-fluorescence in situ hybridization for chromosome karyotyping. *Nat. Protoc.* **1**, 1172–1184 (2006).
21. R. Caeser, *et al.*, Genetic modification of primary human B cells to model high-grade lymphoma. *Nat. Commun.* **10**, 4543 (2019).